

Diversifying NMR Supersequences with New HSQC-Based Modules

Jonathan R. J. Yong,¹ [...?], Ēriks Kupče,² Tim D. W. Claridge^{1,*}

¹ Chemistry Research Laboratory, Department of Chemistry, University of Oxford, Mansfield Road, Oxford, OX1 3TA, U.K.

² Bruker UK Ltd., Banner Lane, Coventry, CV4 9GH, U.K.

* tim.claridge@chem.ox.ac.uk

Abstract

The sensitivity-enhanced HSQC, as well as HSQC-TOCSY, experiments can be incorporated into NOAH (NMR by Ordered Acquisition using ¹H detection) supersequences. Importantly, these heteronuclear modules preserve the magnetisation required for subsequent acquisition of other homonuclear modules in the supersequence. With these new modules, we reach a total of over 600 practically applicable NOAH supersequences which yield high-quality 2D spectra with greatly reduced experiment durations.

In recent years, there has been significant interest in techniques which accelerate the acquisition of NMR data, especially for multidimensional spectra.^{1–3} Some of the more readily implemented approaches involve the use of multiple-FID acquisitions, using either single or multiple receivers. Of these, one of the most versatile approaches is to utilise different “pools” of magnetisation for the sequential collection of different spectra without an intervening recovery delay, as illustrated by the NOAH (NMR by Ordered Acquisition using ¹H detection) technique.⁴ Virtually all of the most common 2D experiments used in small molecule characterisation, such as HMBC, HSQC, COSY, NOESY, and TOCSY, can be concatenated in a modular fashion to form *supersequences* which collectively use only one recovery delay (d_1) (Figure 1a). As the recovery delay accounts for the large majority of experiment time in 2D NMR, the NOAH approach can provide time savings of up to $\sim 4\times$ compared to the conventional individual acquisition of each spectrum, in which each

constituent experiment would require its own recovery delay.

One-bond heteronuclear correlation experiments, namely HSQC and HMQC, play a central role in the structural elucidation of small organic molecules and biomolecules.⁵ These experiments are also a core component of many NOAH experiments, since the magnetisation they use (protons directly coupled to isotopically dilute X nuclei, i.e. ¹³C or ¹⁵N) can be efficiently differentiated from the “bulk” magnetisation of protons that are not directly attached to these NMR-active nuclei.^{4d,6} Following the notation of Orts,⁷ we refer to these two magnetisation components (proton coupled to X and proton not coupled to X) as ¹H^X and ¹H^{!X} respectively. At the same time, due to the low natural abundance of these heteronuclei, these spectra are typically less sensitive than the homonuclear spectra that are placed towards the end of the supersequence. Consequently, for dilute samples, the minimum experimental time is generally dictated by these heteronuclear experiments, meaning any improvements in experiment sensitivity can be translated into greater time savings.

In the 1990s, Cavanagh, Rance, and Kay introduced the sensitivity-enhanced HSQC (seHSQC) experiment, which improves on the sensitivity of an ordinary echo-antiecho HSQC by up to a factor of 2.⁸ This is accomplished by converting two magnetisation components that are cosine- and sine-modulated in t_1 into observable magnetisation prior to detection, in the so-called preservation of equivalent pathways (PEP) scheme. Here, we show how the original seHSQC sequence can be modified such that it can be used as a NOAH module. We add further diversification by introducing a HSQC-TOCSY module, derived from the ASAP-HSQC-TOCSY,⁹ that is also compatible with the NOAH strategy. Both of these modules can be inserted either independently or together into NOAH supersequences, allowing large amounts of chemical information to be acquired in short times.

A typical example of a NOAH supersequence is the NOAH-4 MSCN experiment (Figure 1a), which yields ¹⁵N HMQC, ¹³C HSQC, COSY, and NOESY spectra in one single experiment.^{4a} The implementation of this supersequence relies on the fact that the output of any one module contains all the necessary magnetisation components required for downstream modules. For example, both the standard NOAH HMQC (Figure 1b) and HSQC (Figure 1c) modules return the bulk mag-

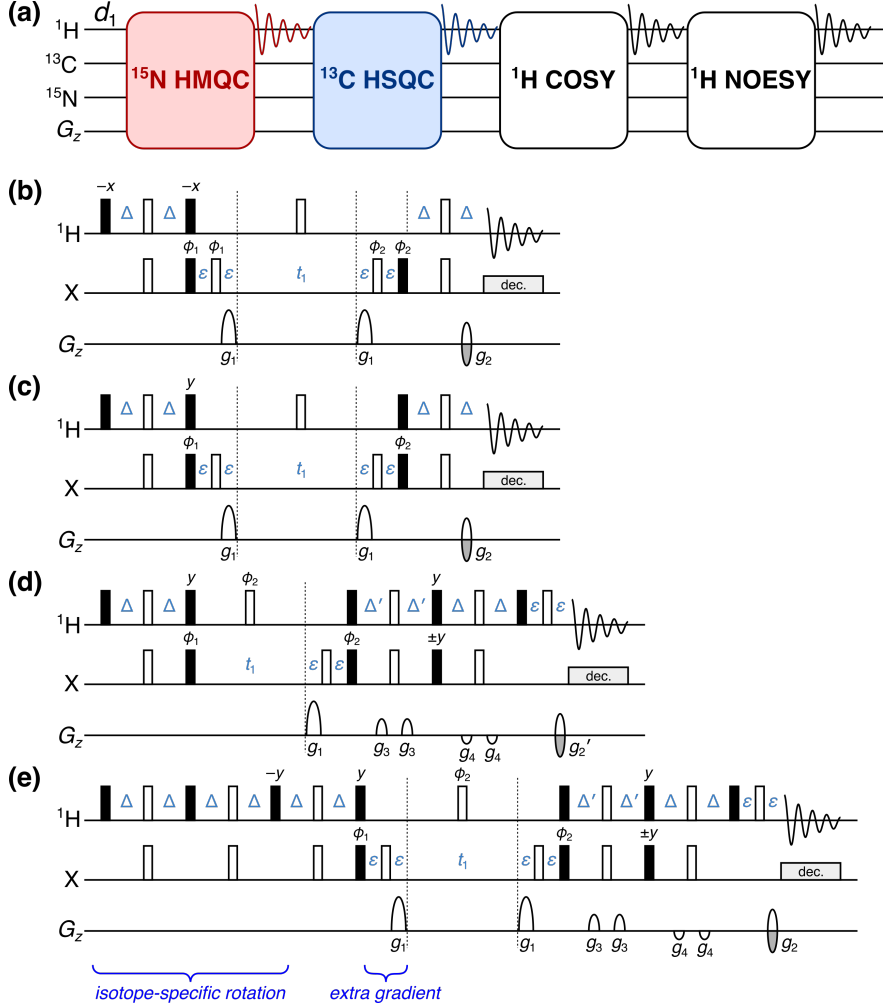


Figure 1: (a) Overview of a typical NOAH supersequence (MSCN, using the single-letter abbreviations previously defined^{4a}). The ^{15}N – ^1H HMQC and ^{13}C – ^1H HSQC modules are coloured; these may be replaced with the new seHSQC module proposed in this work. (b) NOAH HMQC module,^{4a,10} abbreviated as “M”. (c) NOAH HSQC module without sensitivity enhancement,^{4a,11} abbreviated as “S”. (d) Cavanagh–Rance–Kay (CRK) seHSQC.⁸ (e) NOAH seHSQC module, abbreviated as “S⁺” (this work). Filled and unfilled bars represent 90° and 180° pulses respectively; all 180° pulses on ^{13}C are adiabatic (swept-frequency) pulses. All pulses are applied along $+x$ unless otherwise noted. Phase cycling is performed with $\phi_1 = (x, -x)$ and $\phi_2 = (x, x, -x, -x)$. The delays are chosen as follows: $\Delta = 1/(4 \cdot {}^1J_{\text{NH}})$, $\Delta' = 1/(8 \cdot {}^1J_{\text{CH}})$ or $1/(4 \cdot {}^1J_{\text{NH}})$, and ε is the minimum time needed for a gradient pulse and subsequent recovery. All gradient pulses are 1 ms long, except for g_1 and g_2 in ^{15}N experiments which are 2.5 ms long. Gradient amplitudes, as percentages of maximum gradient strength, are as follows: $g_1 = 80\%$; $g_2 = \pm 40.2\%$ (^{13}C) or $\pm 16.2\%$ (^{15}N); $g_2' = g_2/2$; $g_3 = 11\%$; $g_4 = -5\%$. The signs of g_2 and g_2' , as well as the phase of the ^{13}C pulse marked $\pm y$, are alternated within each t_1 increment to provide echo–antiecho selection. Refer to Figure S1 for product operator analysis.

netisation back to its equilibrium position ($+z$). In the MSCN sequence, this bulk magnetisation can therefore be used as the input to the COSY and NOESY homonuclear modules which follow. However, the original Cavanagh–Rance–Kay (CRK) seHSQC (Figure 1d) does not obey this prin-

ciple: it causes bulk magnetisation to be dephased by coherence transfer pathway (CTP) gradients. Consequently, downstream modules can only utilise any bulk $^1\text{H}^{13}\text{C}$ magnetisation that has relaxed during the HSQC FID acquisition, leading to drastic losses in signal intensity. This is illustrated using a NOAH-2 S^+C^c (seHSQC + CLIP-COSY¹²) supersequence (Figure 2a): while the CRK seHSQC implementation afford significant sensitivity gains (primarily for CH peaks, as predicted by theory¹³), the COSY module which follows suffers from an almost complete ($\sim 90\%$) loss of intensity. While one could argue that this is still tolerable for the COSY module, which is the most sensitive of all NOAH modules, these losses are not permissible for less inherently sensitive homonuclear modules such as NOESY and ROESY.

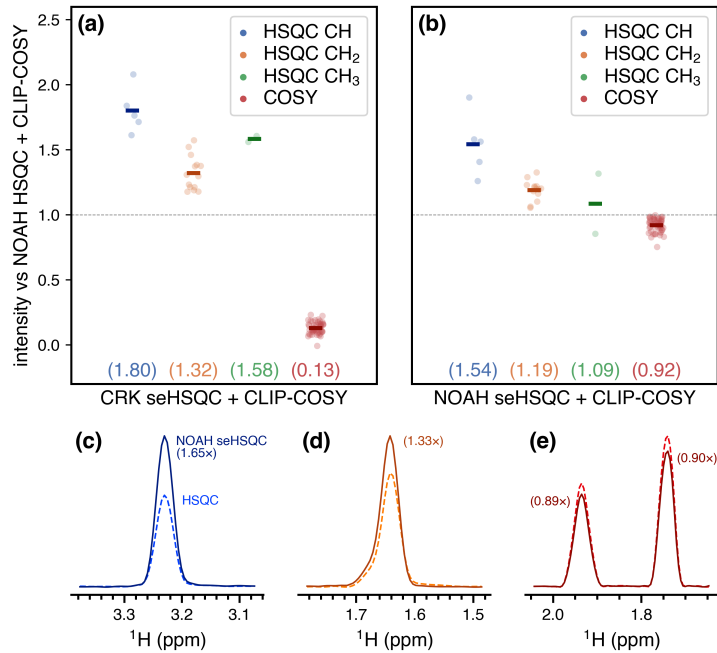


Figure 2: Sensitivity comparisons for NOAH-2 S^+C^c (seHSQC + CLIP-COSY) supersequences, using the CRK (Figure 1d) and NOAH (Figure 1e) seHSQC implementations. The delay Δ' was set to $1/(8 \cdot ^1\text{J}_{\text{CH}})$. All intensities are normalised against the NOAH-2 SC^c (HSQC + CLIP-COSY) supersequence, without HSQC sensitivity enhancement. HSQC intensities are further grouped by multiplicity. Circles represent the relative intensities of individual peaks; solid bars, as well as the numbers in parentheses, indicate averages over all peaks of a given type. (a) Using the original CRK seHSQC. The CRK seHSQC does not preserve the bulk magnetisation, leading to severely reduced COSY intensities. (b) Using the NOAH seHSQC. (c) Slices of the NOAH HSQC (dashed line) and NOAH seHSQC spectra (solid line) through $f_1 = 78.9$ ppm (a CH peak). (d) Slices of the NOAH HSQC (dashed line) and NOAH seHSQC spectra (solid line) through $f_1 = 28.5$ ppm (a CH₂ peak). (e) Slices of the CLIP-COSY module in a NOAH-2 SC^c supersequence (dashed line) and NOAH-2 S^+C^c (solid line) through $f_1 = 1.36$ ppm. Spectra were obtained on a 700 MHz Bruker AV III equipped with a TCI H/C/N cryoprobe; the sample used was 40 mM andrographolide in DMSO-*d*₆.

The solution to this is based on the simple observation that the bulk magnetisation in the seHSQC will be returned to $+z$ if the phase of the initial ${}^1\text{H}$ 90°_x pulse is changed by 90° to $+y$. To generate the required HSQC signal, however, the same pulse needs to be applied along $+x$. Overall, what is required is therefore a pulse sequence element which simultaneously acts as a 90°_x (or 90°_{-x}) pulse on protons coupled to ${}^{13}\text{C}$, and as a 90°_y pulse on uncoupled protons. We accomplish this by prepending a double heteronuclear spin echo, which we herein refer to as the *isotope-specific rotation* (ISR), to the pulse sequence. It is similar to the zz -filter, which we have previously used in the NOAH zz -HMBC module to retain the magnetisation of directly coupled protons for a subsequent HSQC module.^{4b,4d} However, the ISR has different pulse phases to this and consequently leads to a different overall outcome, i.e. 90°_{-x} on ${}^1\text{H}^X$ and 90°_y on ${}^1\text{H}^{!X}$. While the BIG-BIRD element developed by Briand and Sørensen¹⁴ is also capable of effecting this, we find that the ISR provides greater signal-to-noise in both the seHSQC itself as well as downstream modules (Figure S5).

In addition to the ISR, the NOAH seHSQC module also contains a CTP gradient prior to the t_1 period (highlighted in Figure 1e). This gradient is not necessary for the seHSQC module itself, but instead serves to suppress artefacts in downstream modules, which would otherwise arise from bulk magnetisation that evolves during either half of the HSQC t_1 period. This then evolves again in the t_1 period of a later homonuclear module (e.g. COSY), resulting in each COSY peak with *indirect-dimension frequency* $f_1 = \Omega_{\text{H}}$ being accompanied by a pair of “wing” artefacts at $f_1 = \Omega_{\text{H}} \pm (\Omega_{\text{H}} \cdot \text{SW}_{\text{cosy}}) / (2 \cdot \text{SW}_{\text{HSQC}})$, where Ω_{H} and SW refer to the proton offset and indirect-dimension spectral width respectively (both in Hz). Importantly, the artefacts arising from diagonal peaks can have intensities that are comparable to genuine crosspeaks (Figure S6), which highlights the importance of suppressing these artefacts. We also briefly note here that the presence of two CTP gradients inside the seHSQC t_1 period allows the final CTP gradient (g_2) to have twice its usual amplitude, thereby providing additional artefact suppression in the seHSQC itself. This is particularly important in the ${}^{15}\text{N}-{}^1\text{H}$ seHSQC, as will be explained below.

With these modifications, the NOAH seHSQC module provides clear sensitivity gains over the NOAH HSQC module, while preserving essentially the same amount of ${}^1\text{H}$ magnetisation ($\sim 90\%$) for downstream modules (Figure 2b). The modifications present in the NOAH seHSQC, particularly

the ISR, mean that the sensitivity improvements are slightly lower as compared to the original CRK implementation. For this example, CH and CH₂ peaks have an average of 1.54× and 1.19× increased sensitivity respectively relative to the NOAH HSQC module (Figure 2c–d). However, a dramatic improvement is seen in the COSY module which follows. In contrast to the CRK seHSQC, which largely destroys the requisite bulk magnetisation, the NOAH seHSQC preserves the majority of it, performing 92% as well as the original HSQC module (Figure 2e).

Multiplicity editing can be easily incorporated into the NOAH seHSQC sequence (Figure S2), leading to similar sensitivity gains relative to the HSQC module. It is noteworthy that the original NOAH HSQC (without sensitivity enhancement) places the bulk magnetisation in the *xy*-plane during the *t*₁ and editing periods, whereas the newly proposed NOAH seHSQC places the bulk along ±*z*. In the former, the bulk magnetisation is therefore subject to homonuclear coupling (*J*_{HH}) evolution, leading to a small decrease in the sensitivity of later homonuclear modules when multiplicity editing is introduced. Since homonuclear experiments typically have a greater inherent sensitivity than the HSQC, this minor loss is rarely a problem, and is far outweighed by the benefits of incorporating multiplicity editing in the HSQC. Nevertheless, the fact that the seHSQC does not suffer from such a penalty is a welcome benefit. As a result, the edited NOAH seHSQC slightly outperforms the edited HSQC in terms of preserving bulk magnetisation, with subsequent homonuclear modules enjoying a small sensitivity boost of around 10% (Figure S3).

The proposed seHSQC module can be similarly implemented for ¹⁵N experiments. Currently, in NOAH supersequences, ¹⁵N–¹H correlations are primarily obtained using the HMQC module,^{4a,10} since this manipulates bulk ¹H!¹⁵N magnetisation more favourably than the HSQC (*vide infra*; see also Figure S1). Compared to this, the new seHSQC module can provide greater than 4× enhanced sensitivity (Figure 3). This arises partly because the PEP sensitivity enhancement scheme can be optimised for NH peaks by setting the reverse INEPT transfer delay Δ' to be equal to 1/(4 · ¹*J*_{NH}). However, there is also a significant improvement due to the fact that peaks in the ¹⁵N seHSQC are not broadened in the indirect dimension by *J*_{HH}, unlike in the ¹⁵N HMQC. Although the seHSQC retains a slightly smaller amount of ¹H!¹⁵N magnetisation (~ 70%, versus ~ 80% for the HMQC (Figure S8)), this is almost never a problem, since it is the ¹⁵N module which typically has the

lowest intrinsic sensitivity in a supersequence.

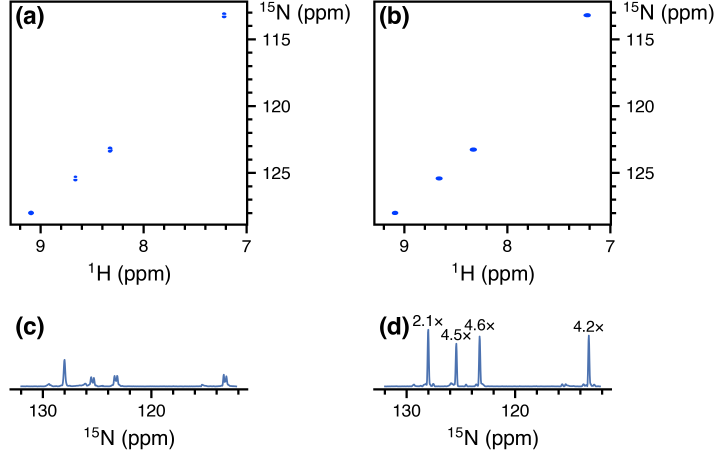


Figure 3: Comparison of the new ^{15}N - ^1H seHSQC with the standard NOAH HMQC module, taken from NOAH-3 XS $^+ \text{C}^\text{c}$ supersequences (^{15}N experiment + ^{13}C seHSQC + CLIP-COSY). (a) ^{15}N HMQC spectrum. (b) ^{15}N seHSQC spectrum. (c) Projection of HMQC onto the f_1 axis. Splitting due to J_{HH} is clearly visible for three of the four peaks. (d) Projection of seHSQC onto the f_1 axis. Signal-to-noise improvements relative to the HMQC spectrum are indicated over each peak. The largest gains are observed for peaks where the multiplet structure is collapsed; however, even in the absence of that, a $\sim 2\times$ gain is still obtained. Spectra were obtained on a 700 MHz Bruker AV III equipped with a TCI H/C/N cryoprobe; the sample used was 40 mM gramicidin in DMSO- d_6 .

While a ^{15}N HSQC module (without sensitivity enhancement) would still benefit from multiplet collapse, it comes with other severe drawbacks. As previously discussed, the HSQC module places bulk $^1\text{H}^{1\text{N}}$ magnetisation in the xy -plane during the t_1 period. Consequently, the amount of bulk magnetisation that is retained decreases as t_1 is lengthened, leading to line broadening in the indirect dimensions of all downstream modules (Figure S9). Whilst this is not a problem with the ^{13}C HSQC where typical ^{13}C indirect dimension acquisition times are relatively short, the smaller spectral widths in ^{15}N experiments can mean downstream modules suffer moderate losses in both sensitivity and resolution. The seHSQC module avoids this issue entirely, making it especially well-suited to obtaining ^{15}N correlations.

A potential issue in the ^{15}N seHSQC module arises from the cumulative effects of pulse imperfections, which cause a portion of bulk $^1\text{H}^{1\text{N}}$ magnetisation to be transverse just prior to detection of the seHSQC signal. Although this only represents a small fraction of the bulk magnetisation, if left uncontrolled, the resulting artefacts typically have intensities that are comparable to the seHSQC

crosspeaks (Figure S10). The key to suppressing these artefacts efficiently lies in the final CTP gradient g_2 (Figure 1e), which dephases any transverse bulk magnetisation. The NOAH seHSQC therefore greatly benefits from having two CTP gradients g_1 within the t_1 period, as this means that g_2 will have twice its usual amplitude. For optimal performance, however, the ^{15}N seHSQC module should be modified in one other respect: the CTP gradients g_1 and g_2 should all be lengthened from their typical duration of 1 ms, in order to provide more effective dephasing. In practice, we find that gradient durations of 2 to 2.5 ms provide excellent artefact suppression whilst not causing any appreciable difference in the intensity of the desired crosspeaks (Figure S10). These extended gradients are not required in the ^{13}C seHSQC for two reasons: firstly, the amplitude of g_2 in the ^{13}C seHSQC is larger by a factor of $\gamma_{\text{C}}/\gamma_{\text{N}} \approx 2.5$; and secondly, the greater natural abundance of ^{13}C (1.1% versus 0.36% of ^{15}N) leads to a larger signal intensity.

In scenarios where high resolution in the ^{15}N dimension is not required, it can prove useful to reduce the number of t_1 increments and in its place increase the number of transients acquired.^{2b,15} In new versions of the NOAH pulse programmes (including those provided in the *Supporting Information*), this feature can be enabled by specifying a factor k by which to perform this scaling. Note that the scaling is only applied to the ^{15}N module; all other modules are left untouched. In our hands, setting $k = 2$ or 4 for the original ^{15}N HMQC can lead to significant sensitivity gains of up to $\sim 2\times$, since J_{HH} splitting in the indirect dimension can no longer be resolved (Figure S11). This point is not relevant to the seHSQC, and here k -scaling on its own has only a tiny effect on peak height (and signal-to-noise), since any sensitivity gained from the extra transients is typically offset by the broadening (Figure S12). However, the later t_1 increments which were not acquired can be reconstructed using linear projection¹⁶ to mitigate this line broadening. The resulting spectra display sensitivity gains of up to a factor of k , although the fidelity of the reconstruction can suffer for large k , particularly with the HMQC (Figures S13–S14).

Next, we note that the HSQC module (though not the new seHSQC module) allows an arbitrary amount of $^{1}\text{H}^{\text{C}}$ magnetisation to be excited, with the remainder returned to $+z$. In order to excite a proportion f of $^{1}\text{H}^{\text{C}}$ magnetisation ($0 < f \leq 1$), the initial INEPT delay must be shortened by a factor of $\sin^{-1} f$. The remaining $(1 - f)$ of the magnetisation, plus any that relaxes during

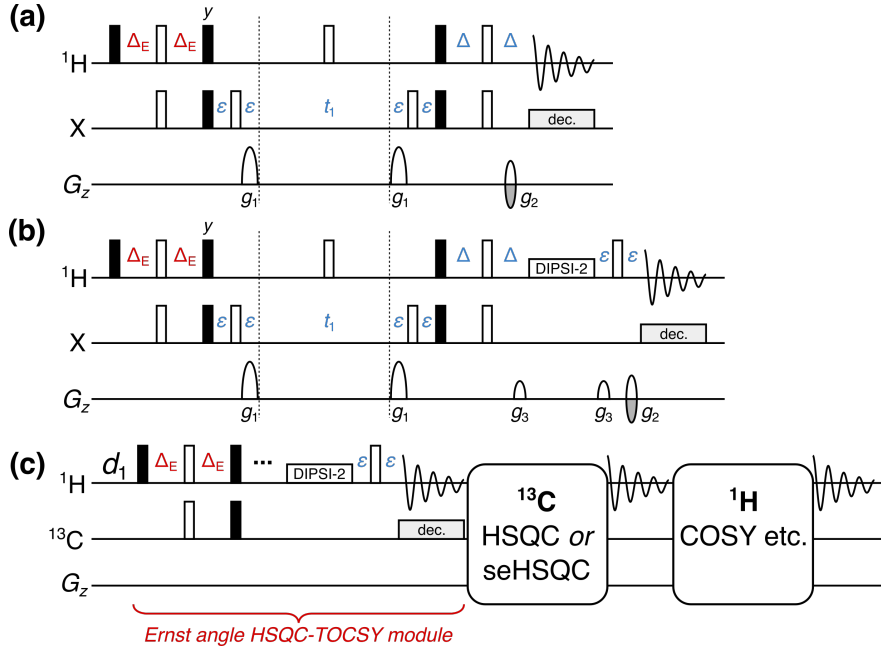


Figure 4: (a) NOAH HSQC module with modified INEPT delay $\Delta_E = (\sin^{-1} f)/(4 \cdot {}^1J_{\text{CH}})$, where f is the fraction of ${}^{13}\text{C}$ - ${}^1\text{H}$ magnetisation excited. (b) NOAH HSQC-TOCSY module (“S^T”), modified from the ASAP-HSQC-TOCSY.⁹ The gradients g_3 are 1 ms long, and are set to 19% of the maximum gradient amplitude. (c) Overview of a NOAH-3 S^TSX or S^TS⁺X supersequence. The ${}^{13}\text{C}$ - ${}^1\text{H}$ magnetisation is partly used by the initial HSQC-TOCSY module, with a subsequent HSQC or seHSQC using the remaining magnetisation. The bulk magnetisation is retained for one or more homonuclear modules at the end. All other symbols have the same meanings as in Figure 1.

the HSQC FID, can then be used for a *second* HSQC-based module in the same supersequence. Such a scheme proves to be useful for simultaneously collecting ${}^{13}\text{C}$ -decoupled and coupled HSQC spectra, or HSQC spectra with different spectral widths. This has previously been accomplished in a multi-FID acquisition (MFA) scheme by keeping the two CTPs in the CRK seHSQC separate, with the cosine- and sine-modulated CTPs each contributing to one spectrum.¹⁷ With the present NOAH strategy, for values of f that are close to 1, the amount of ${}^1\text{H}^{\text{C}}$ magnetisation regained through relaxation can reach almost 50%. Consequently, by setting $f \approx 0.8$, we can obtain two HSQC spectra with sensitivities that are comparable to the existing MFA approach. Furthermore, the sensitivity of the second HSQC can be boosted by using the new seHSQC module in its place (Figure S15).

By adding a period of isotropic mixing prior to detection, the NOAH HSQC module may be converted to a HSQC-TOCSY module (denoted by “S^T”). This is similar to the previously reported

ASAP-HSQC-TOCSY,⁹ the key difference being that in the present NOAH context, unused ¹H¹³C as well as bulk ¹H¹³C magnetisation is preserved for use in other modules, instead of later t_1 increments as in the ASAP experiment. Compared to the existing MFA HSQC-TOCSY/HSQC experiment,^{17a} our approach has several characteristics which make it particularly amenable to use in NOAH supersequences. Firstly, the vast majority of ¹H¹³C magnetisation is preserved, as required for homonuclear module(s) to be appended in a NOAH supersequence (in practice, losses of ca. 10% are observed due to pulse imperfections). In contrast, the MFA sequence, much like the original CRK seHSQC on which it is based, dephases ¹H¹³C magnetisation and causes a 80–90% sensitivity loss in downstream spectra. Secondly, the sensitivity of both spectra in a NOAH experiment can be optimised through the value of f ; this allows a larger amount of ¹³C–¹H magnetisation to be used for the inherently less sensitive HSQC-TOCSY. In our experience, setting $f = 0.9$ provides a good balance for S^TS combinations: the sensitivity in the HSQC is boosted not only by relaxation during the HSQC-TOCSY FID, but also by the isotropic mixing in the HSQC-TOCSY module, which effects a degree of ¹H¹³C → ¹H¹³C magnetisation transfer (Figure S16). Lastly, since each NOAH module is independently executed, the NOAH approach allows multiplicity editing to be enabled for only the HSQC and not the HSQC-TOCSY, where accidental overlap may lead to crosspeaks being lost unexpectedly. Despite these benefits, we note that it is not possible to simply insert a TOCSY mixing block into the seHSQC module presented here, as that will lead to the bulk ¹H¹³C magnetisation being dephased. Therefore, the NOAH HSQC-TOCSY module will still have lower overall sensitivity than a conventional seHSQC-TOCSY which makes use of the PEP scheme.

There exist many ways in which the new modules discussed above can be included in practical experiments for structure characterisation. Here, we illustrate this with the NOAH-4 S_N⁺S^TS⁺C^c (¹⁵N seHSQC, ¹³C HSQC-TOCSY, ¹³C seHSQC, and CLIP-COSY) supersequence (Figure 5). While individual collection of the four spectra above would require 57 minutes and 8 seconds, the NOAH-4 supersequence takes only 17 minutes and 35 seconds; this is 30.8% of the original duration, or equivalently a 3.25× speedup. For typical organic molecules, new supersequences such as the NOAH-4 S^TS⁺CT allow the rapid and complete collection of C–H and H–H correlations (Figure S17). Experiment times can be further reduced through the use of non-uniform sampling (Figure

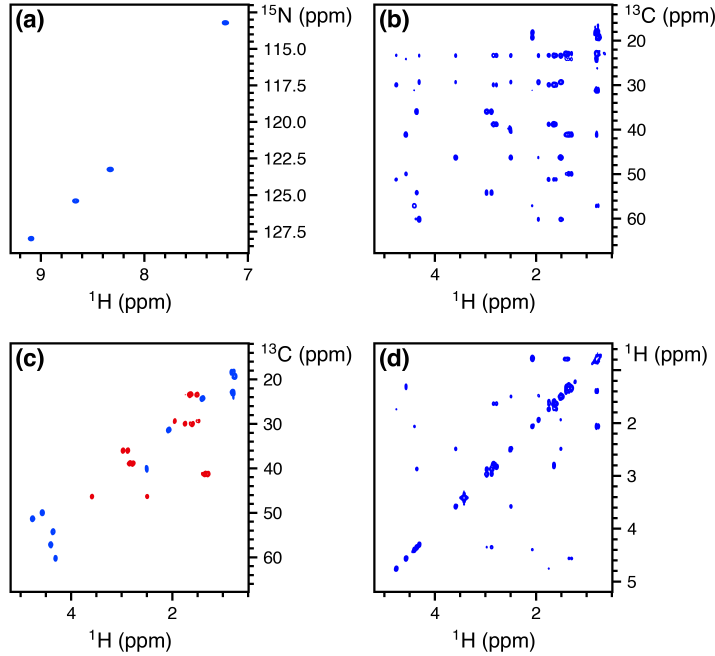


Figure 5: Spectra obtained from the NOAH-4 $S_N^+S^TS^+C^c$ supersequence. 256 t_1 increments were used, with 2 scans per increment. The total experiment time was 17 minutes and 35 seconds. (a) ^{15}N seHSQC. (b) ^{13}C HSQC-TOCSY (30 ms mixing, $f = 0.9$). (c) Multiplicity-edited ^{13}C seHSQC. Notice that having the edited seHSQC removes the need for the less desirable HSQC-TOCSY editing. (d) CLIP-COSY. Spectra were obtained on a 700 MHz Bruker AV III equipped with a TCI H/C/N cryoprobe; the sample used was 40 mM gramicidin (a cyclic decapeptide; (Val–Orn–Leu–D-Phe–Pro)₂) in DMSO- d_6 .

S18), which is compatible with nearly all of the supersequences shown here. One can also prepend the NOAH zz -HMBC module (“B”);^{4d} this uses the semi-adiabatic zz -filter to preserve both $^1\text{H}^C$ and $^1\text{H}^N$ magnetisation, which can then be sampled in the HSQC-based modules presented here (Figure S19).

The new seHSQC and HSQC-TOCSY implementations add to the preexisting diversity in NOAH modules, bringing the total number of plausible NOAH supersequences to over 600. The AU scripts needed for processing of these modules, as well as a number of the more commonly used pulse sequences, are provided in the *Supporting Information*; others are available upon request from the authors. However, a more user-friendly and customisable method for the generation of NOAH pulse sequences is clearly needed to handle the sheer variety currently available. Our work towards this will be reported in the near future.

Acknowledgements

J.R.J.Y. thanks the Clarendon Fund (University of Oxford) and the EPSRC Centre for Doctoral Training in Synthesis for Biology and Medicine (EP/L015838/1) for a studentship, generously supported by AstraZeneca, Diamond Light Source, Defence Science and Technology Laboratory, Evotec, GlaxoSmithKline, Janssen, Novartis, Pfizer, Syngenta, Takeda, UCB, and Vertex. ...

References

1. (a) Frydman, L.; Scherf, T.; Lupulescu, A. *Proc. Natl. Acad. Sci. U. S. A.* **2002**, *99*, 15858–15862; (b) Frydman, L.; Lupulescu, A.; Scherf, T. *J. Am. Chem. Soc.* **2003**, *125*, 9204–9217.
2. (a) Nolis, P.; Pérez-Trujillo, M.; Parella, T. *Angew. Chem. Int. Ed.* **2007**, *46*, 7495–7497; (b) Parella, T.; Nolis, P. *Concepts Magn. Reson.* **2010**, *36A*, 1–23.
3. (a) Kupče, Ē.; Freeman, R.; John, B. K. *J. Am. Chem. Soc.* **2006**, *128*, 9606–9607; (b) Kovacs, H.; Kupče, Ē. *Magn. Reson. Chem.* **2016**, *54*, 544–560.
4. (a) Kupče, Ē.; Claridge, T. D. W. *Angew. Chem. Int. Ed.* **2017**, *56*, 11779–11783; (b) Kupče, Ē.; Claridge, T. D. W. *Chem. Commun.* **2018**, *54*, 7139–7142; (c) Claridge, T. D. W.; Mayzel, M.; Kupče, Ē. *Magn. Reson. Chem.* **2019**, *57*, 946–952; (d) Kupče, Ē.; Claridge, T. D. W. *J. Magn. Reson.* **2019**, *307*, 106568.
5. (a) Claridge, T. D. W., *High-Resolution NMR Techniques in Organic Chemistry*, 3rd ed.; Elsevier: Amsterdam, 2016; (b) Cavanagh, J., *Protein NMR Spectroscopy: Principles and Practice*, 2nd ed.; Academic Press: Burlington, Mass., 2007.
6. Garbow, J. R.; Weitekamp, D. P.; Pines, A. *Chem. Phys. Lett.* **1982**, *93*, 504–509.
7. Orts, J.; Gossert, A. D. *Methods* **2018**, *138–139*, 3–25.
8. (a) Palmer, A. G.; Cavanagh, J.; Wright, P. E.; Rance, M. *J. Magn. Reson.* **1991**, *93*, 151–170; (b) Kay, L.; Keifer, P.; Saarinen, T. *J. Am. Chem. Soc.* **1992**, *114*, 10663–10665; (c) Cavanagh, J.; Rance, M. *Annu. Rep. NMR Spectrosc.* **1993**, *27*, 1–58.
9. Becker, J.; Koos, M. R. M.; Schulze-Sünninghausen, D.; Luy, B. *J. Magn. Reson.* **2019**, *300*, 76–83.

10. Kupče, Ē.; Freeman, R. *Magn. Reson. Chem.* **2007**, *45*, 2–4.
11. Schulze-Sünninghausen, D.; Becker, J.; Koos, M. R. M.; Luy, B. *J. Magn. Reson.* **2017**, *281*, 151–161.
12. Koos, M. R. M.; Kummerlöwe, G.; Kaltschnee, L.; Thiele, C. M.; Luy, B. *Angew. Chem. Int. Ed.* **2016**, *55*, 7655–7659.
13. (a) Schleucher, J.; Schwendinger, M.; Sattler, M.; Schmidt, P.; Schedletzky, O.; Glaser, S. J.; Sørensen, O. W.; Griesinger, C. *J. Biomol. NMR* **1994**, *4*, 301–306; (b) Kontaxis, G.; Stonehouse, J.; Laue, E. D.; Keeler, J. *J. Magn. Reson.* **1994**, *111*, 70–76.
14. Briand, J.; Sørensen, O. W. *J. Magn. Reson.* **1997**, *125*, 202–206.
15. Pérez-Trujillo, M.; Nolis, P.; Bermel, W.; Parella, T. *Magn. Reson. Chem.* **2007**, *45*, 325–329.
16. (a) Tufts, D.; Kumaresan, R. *IEEE Trans. Acoust., Speech, Signal Process.* **1982**, *30*, 671–675; (b) Koehl, P. *Prog. Nucl. Magn. Reson. Spectrosc.* **1999**, *34*, 257–299.
17. (a) Nolis, P.; Motiram-Corral, K.; Pérez-Trujillo, M.; Parella, T. *ChemPhysChem* **2019**, *20*, 356–360; (b) Nolis, P.; Motiram-Corral, K.; Pérez-Trujillo, M.; Parella, T. *J. Magn. Reson.* **2019**, *300*, 1–7.

Supporting Information
for
Diversifying NMR Supersequences with New
HSQC-based Modules

Jonathan R. J. Yong,¹ [...?], Ēriks Kupče,² Tim D. W. Claridge^{1,*}

¹ *Chemistry Research Laboratory, Department of Chemistry, University of Oxford,
Mansfield Road, Oxford, OX1 3TA, U.K.*

² *Bruker UK Ltd., Banner Lane, Coventry, CV4 9GH, U.K.*

* tim.claridge@chem.ox.ac.uk

Contents

1 Product operator analysis for NOAH modules	S3
2 Multiplicity editing in seHSQC	S4
3 Effect of setting $\Delta' = 1/(4 \cdot {}^1J_{\text{CH}})$ in seHSQC	S5
4 Comparison of BIG-BIRD and ISR elements	S6
5 Origin and suppression of wing artefacts	S7
6 Retention of bulk magnetisation by ${}^{15}\text{N}$ modules	S10
7 ${}^{15}\text{N}$ HSQC and line broadening	S11
8 Effect of lengthened gradients in ${}^{15}\text{N}$ modules	S12
9 Effect of k-scaling	S13
10 HSQC-TOCSY/HSQC sensitivity comparisons	S18
11 Other example spectra	S21
12 Pulse programmes	S24
13 Processing scripts	S25

1 Product operator analysis for NOAH modules

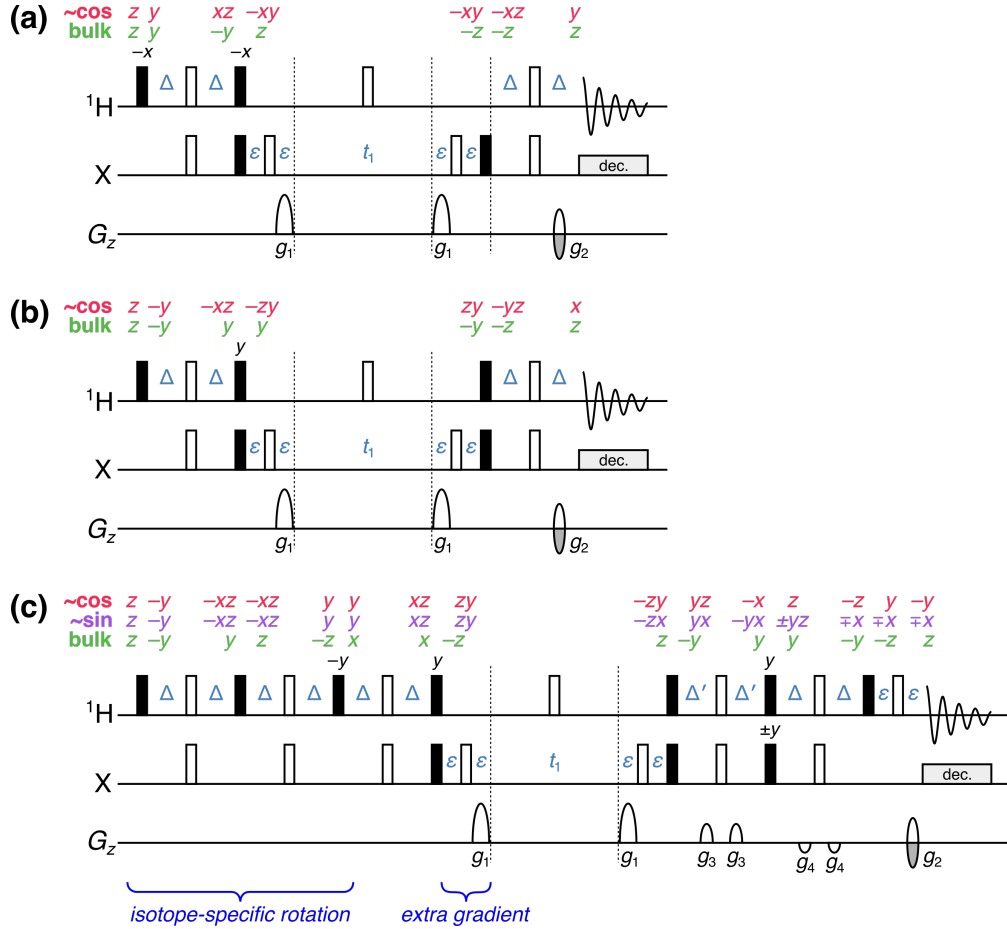


Figure S1: Product operators present at each stage of NOAH modules for an IS spin system. One-letter terms m ($m \in \{x, y, z\}$) are shorthand for single-spin terms on proton, i.e. \hat{I}_m . Two-letter terms mn are shorthand for two-spin terms on both the proton and heteronucleus, i.e. $2\hat{I}_m\hat{S}_n$. “ $\sim\cos$ ” represents the pathway for directly coupled proton magnetisation that is cosine-modulated after t_1 : for the HMQC and HSQC, this is the only component that is detected. For the seHSQC, the sine-modulated component (labelled with “ $\sim\sin$ ”) is also detected. “bulk” refers to the bulk magnetisation, i.e. protons that are not directly coupled to the heteronucleus. (a) NOAH HMQC. (b) NOAH HSQC. (c) NOAH seHSQC with ISR. Immediately following the ISR pulse sequence element, directly bonded protons are rotated onto $+y$, whereas the bulk magnetisation is rotated onto $+x$. Note that this analysis assumes $\Delta = \Delta' = 1/(4 \cdot {}^1J_{\text{XH}})$.

2 Multiplicity editing in seHSQC

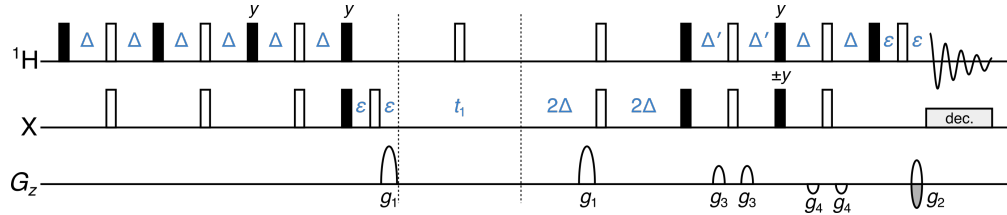


Figure S2: Implementation of multiplicity editing in the new NOAH seHSQC module. Note the different phase in the third ^1H 90° pulse ($+y$ as opposed to the $-y$ in Figure S1c). This is needed to compensate for the extra ^1H 180° pulse in the editing period. Symbols have the same meaning as in Figure 1 of the main text.

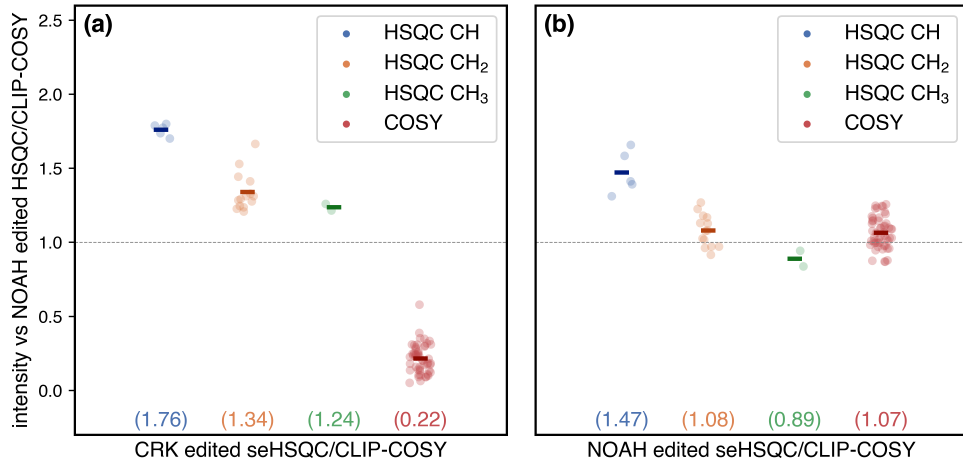


Figure S3: Sensitivity of multiplicity-edited $\text{S}^+\text{C}^{\text{c}}$ supersequence, relative to the SC^{c} supersequence. Spectra were obtained with $\Delta' = 1/(8 \cdot {}^1\text{J}_{\text{CH}})$. (a) CRK edited seHSQC + CLIP-COSY. Although larger gains are observed in the HSQC, the COSY intensities are severely decreased. (b) NOAH edited seHSQC + CLIP-COSY. On average, sensitivity gains are observed in both the HSQC and COSY modules relative to the standard NOAH HSQC (except for HSQC CH₃ peaks). Spectra were obtained on a 700 MHz Bruker AV III equipped with a TCI H/C/N cryoprobe; the sample used was 40 mM andrographolide in DMSO-*d*₆.

3 Effect of setting $\Delta' = 1/(4 \cdot {}^1J_{\text{CH}})$ in seHSQC

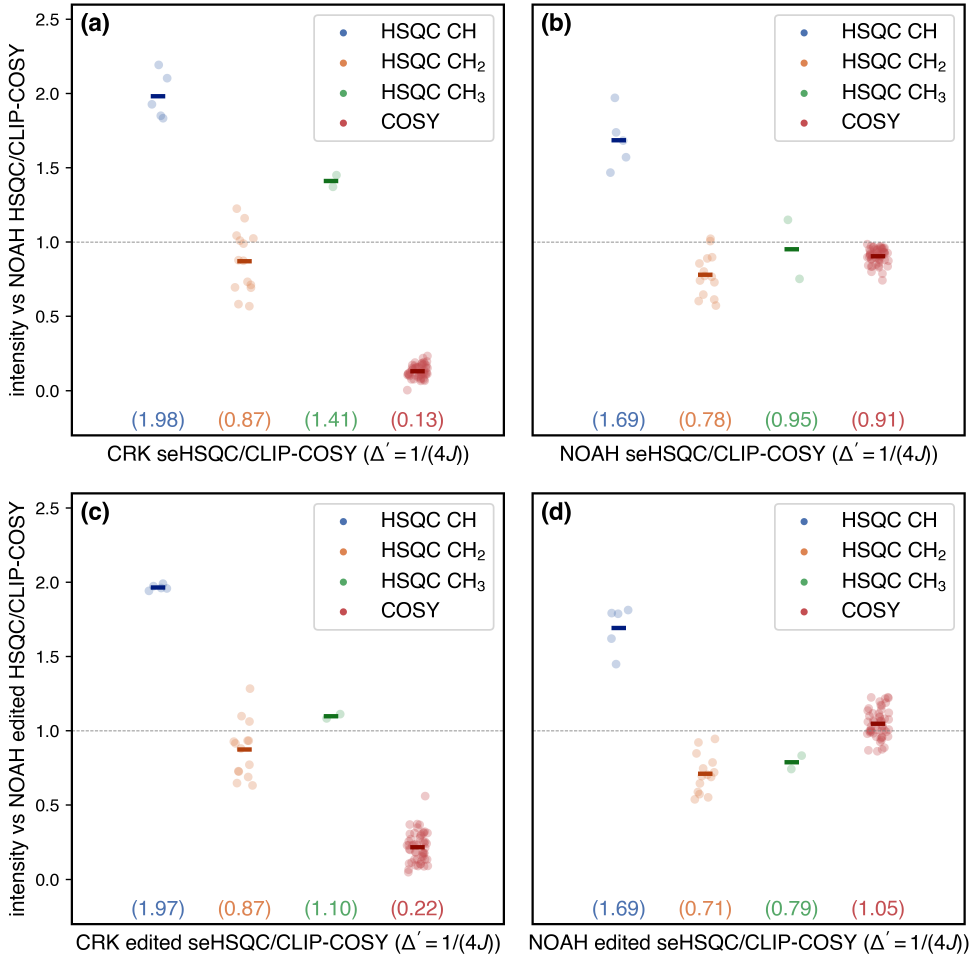


Figure S4: Sensitivity of seHSQC sequences with Δ' set to $1/(4 \cdot {}^1J_{\text{CH}})$, versus the corresponding NOAH HSQC/CLIP-COSY supersequence (i.e. unedited for (a) and (b), edited for (c) and (d)). (a) CRK seHSQC + CLIP-COSY, without multiplicity editing. (b) NOAH seHSQC + CLIP-COSY, without multiplicity editing. (c) CRK seHSQC + CLIP-COSY, with multiplicity editing. (d) NOAH seHSQC + CLIP-COSY, with multiplicity editing. Spectra were obtained on a 700 MHz Bruker AV III equipped with a TCI H/C/N cryoprobe; the sample used was 40 mM andrographolide in DMSO-*d*₆.

By setting $\Delta' = 1/(4 \cdot {}^1J_{\text{CH}})$, theory predicts a larger sensitivity enhancement for CH peaks, whereas CH₂ and CH₃ peaks should have the same sensitivity as in the unenhanced HSQC. However, for the NOAH seHSQC, we note that the improvements in HSQC CH sensitivity gained by moving from $\Delta' = 1/(8 \cdot {}^1J_{\text{CH}})$ (Figure 2b) to $\Delta' = 1/(4 \cdot {}^1J_{\text{CH}})$ (Figure S4b) are marginal (ca. 10%). At the same time, for CH₂ and CH₃ peaks, we observe sensitivity *losses* relative to the HSQC; this is likely due to pulse imperfections in the longer pulse sequence and is in line with previous studies (ref. 13 of the main text).

4 Comparison of BIG-BIRD and ISR elements

The BIG-BIRD element used here was $45^\circ_{45^\circ}(^1\text{H}) - 2\Delta - 180^\circ(^1\text{H}, ^{13}\text{C}) - 2\Delta - 45^\circ_{225^\circ}(^1\text{H})$ for the unedited NOAH seHSQC, where β_ϕ indicates a hard pulse with flip angle β and phase ϕ , and $\Delta = 1/(4 \cdot ^1\text{J}_{\text{CH}})$. For the edited NOAH seHSQC, the BIG-BIRD pulse phases are slightly modified to give $45^\circ_{315^\circ}(^1\text{H}) - 2\Delta - 180^\circ(^1\text{H}, ^{13}\text{C}) - 2\Delta - 45^\circ_{135^\circ}(^1\text{H})$. These, and the ISR, have the same net effect on $^1\text{H}^{\text{C}}$ and $^1\text{H}^{1\text{C}}$ magnetisation, as can be seen from the product operator analysis in Figure S1. However, the ISR provides greater sensitivity in both the HSQC and downstream COSY.

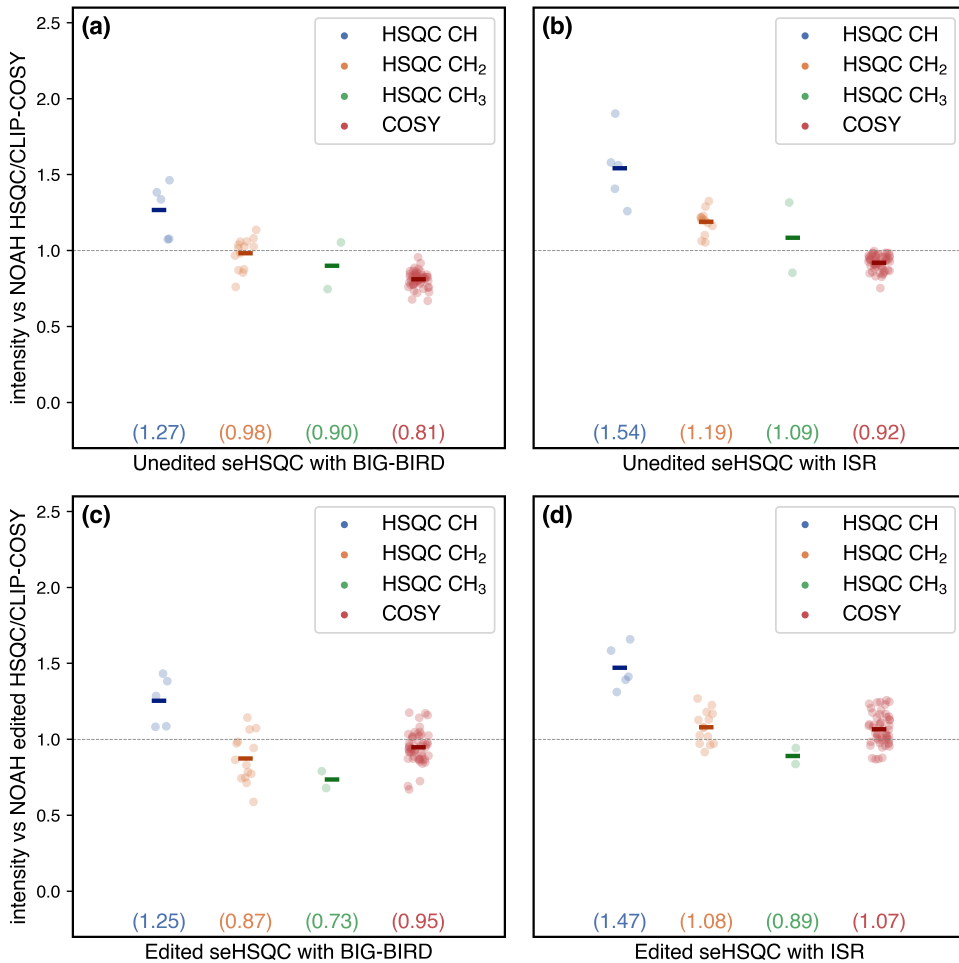


Figure S5: Sensitivity of NOAH-2 S⁺C^c supersequences with either BIG-BIRD or ISR elements, versus the corresponding NOAH-2 SC^c supersequences (i.e. unedited for (a) and (b), edited for (c) and (d)). (a) Using the unedited NOAH seHSQC with the BIG-BIRD element. (b) Unedited seHSQC with ISR. (c) Edited seHSQC with BIG-BIRD. (d) Edited seHSQC with ISR. Spectra were obtained on a 700 MHz Bruker AV III equipped with a TCI H/C/N cryoprobe; the sample used was 40 mM andrographolide in DMSO-*d*₆.

5 Origin and suppression of wing artefacts

The origin of the “wing” artefacts in the final homonuclear modules can be most clearly seen from the following series of experiments involving the NOAH-3 ^{15}N seHSQC/ ^{13}C seHSQC/CLIP-COSY ($\text{S}_\text{N}^+\text{S}^+\text{C}^\text{c}$) supersequence. Since the f_1 spectral windows of the two seHSQC modules are different, they lead to distinct sets of wing artefacts in the COSY if the extra gradient before t_1 is not present. As described in the main text, each peak in the COSY with an indirect-dimension frequency of $f_1 = \Omega_\text{H}$ is flanked by a pair of artefacts at

$$f_1 = \Omega_\text{H} \pm \Omega_\text{H} \cdot \left(\frac{\text{SW}_{\text{COSY}}}{2 \cdot \text{SW}_{\text{HSQC}}} \right),$$

where Ω_H is the offset of the relevant proton and SW refers to the indirect-dimension spectral width. In the spectra shown in the following figures, we have

$$\begin{aligned} \text{SW}_{^{15}\text{N HSQC}} &= 2128 \text{ Hz} \\ \text{SW}_{^{13}\text{C HSQC}} &= 23810 \text{ Hz} \\ \text{SW}_{\text{COSY}} &= 8418 \text{ Hz} \end{aligned}$$

meaning that the artefacts coming from the ^{15}N seHSQC occur at $f_1 = (1.00 \pm 1.98)\Omega_\text{H}$ (and are therefore often folded), whereas artefacts coming from the ^{13}C seHSQC occur at $f_1 = (1.00 \pm 0.18)\Omega_\text{H}$ (and are typically found very close to the main peak). In both cases, the artefacts associated with intense methyl group peaks are the most obvious, but similar artefacts are observed for all other peaks, albeit with lower absolute intensities.

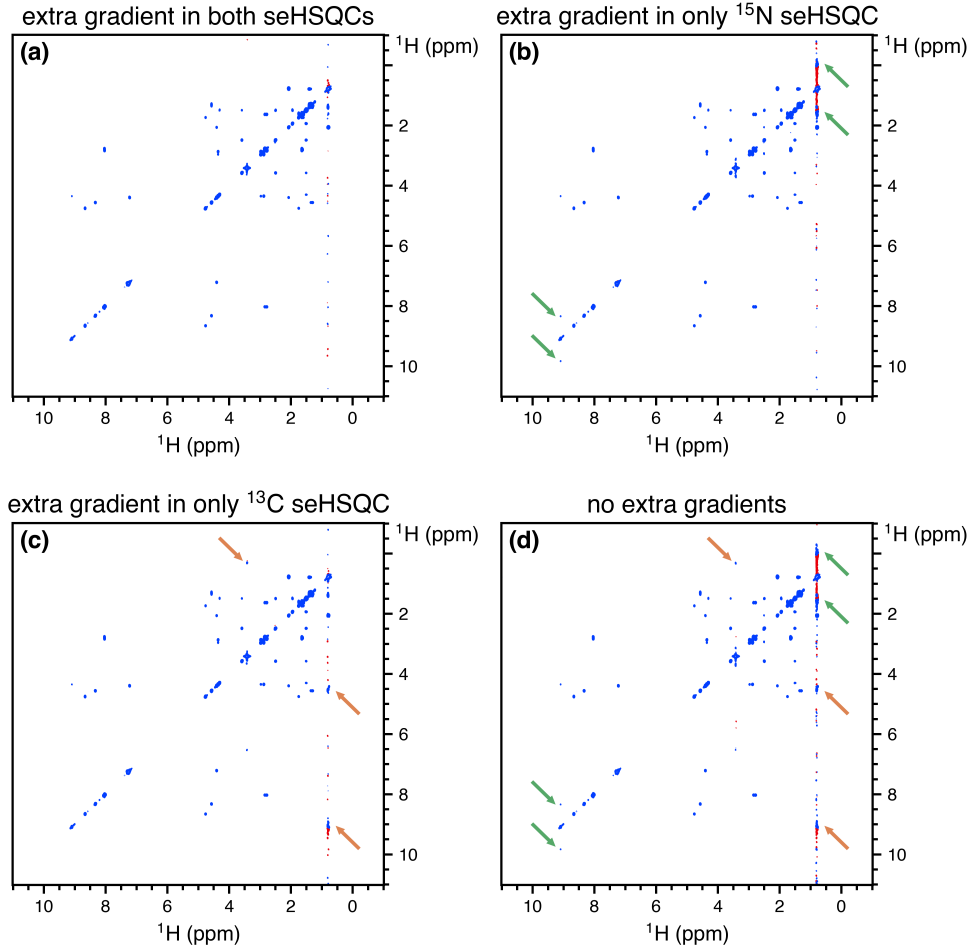


Figure S6: CLIP-COSY spectra obtained from various forms of the NOAH-3 $S_N^+S^+C^c$ supersequence. Wing artefacts arising from the ^{15}N seHSQC are highlighted in orange; those arising from the ^{13}C seHSQC in green. Notice how (in this case) the former can easily be misinterpreted as a crosspeak, while the latter obscures genuine crosspeaks. **(a)** With the extra gradient inserted for both modules, i.e. no artefacts. **(b)** With an extra gradient in only the ^{15}N module, i.e. only the ^{13}C artefacts. **(c)** With an extra gradient in only the ^{13}C module. **(d)** With no extra gradients. Spectra were obtained on a 700 MHz Bruker AV III equipped with a TCI H/C/N cryoprobe; the sample used was 40 mM gramicidin in DMSO- d_6 .

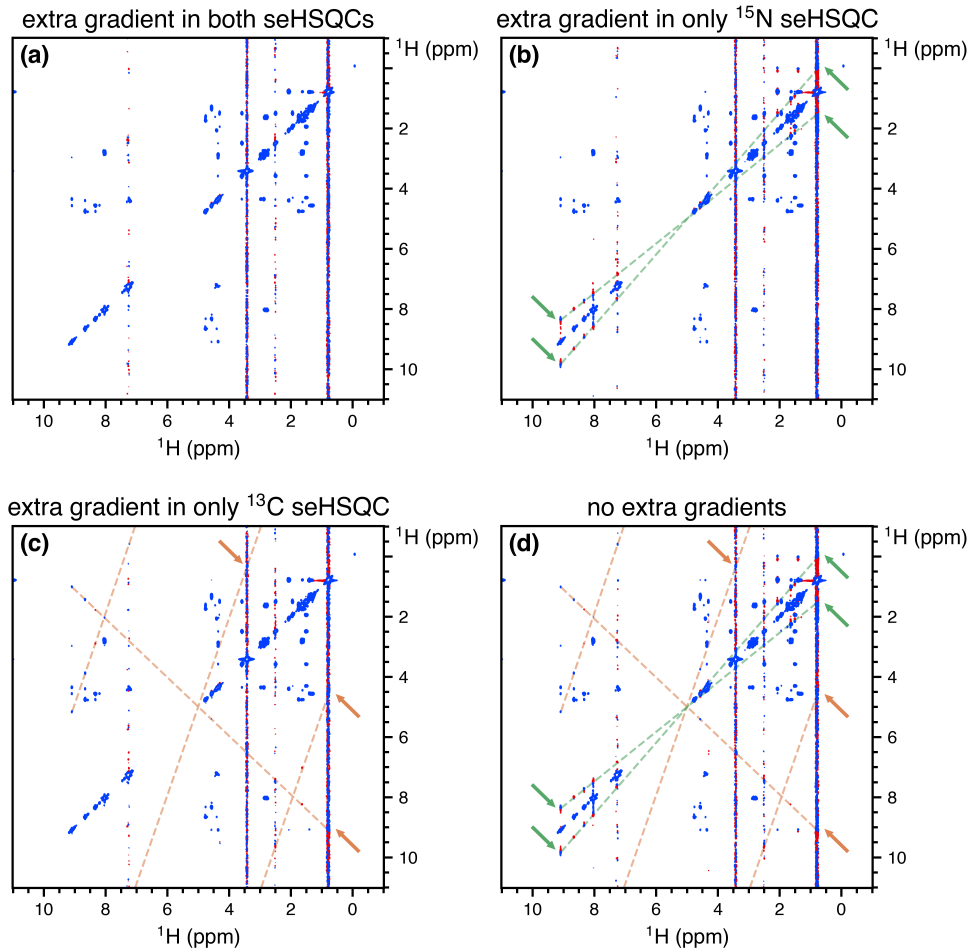


Figure S7: The same as Figure S6, but plotted with a smaller base contour level to illustrate the regular indirect-dimension frequencies of the wing artefacts. A greater number of artefacts are now visible (in addition to those already highlighted in Figure S6, which are still marked with arrows). The artefacts arising from the ^{15}N seHSQC lie on the orange dotted line; those arising from the ^{13}C seHSQC lie on the green dotted line. **(a)** With the extra gradient inserted for both modules, i.e. no artefacts. **(b)** With an extra gradient in only the ^{15}N module, i.e. only the ^{13}C artefacts. **(c)** With an extra gradient in only the ^{13}C module. **(d)** With no extra gradients. Spectra were obtained on a 700 MHz Bruker AV III equipped with a TCI H/C/N cryoprobe; the sample used was 40 mM gramicidin in DMSO- d_6 .

6 Retention of bulk magnetisation by ^{15}N modules

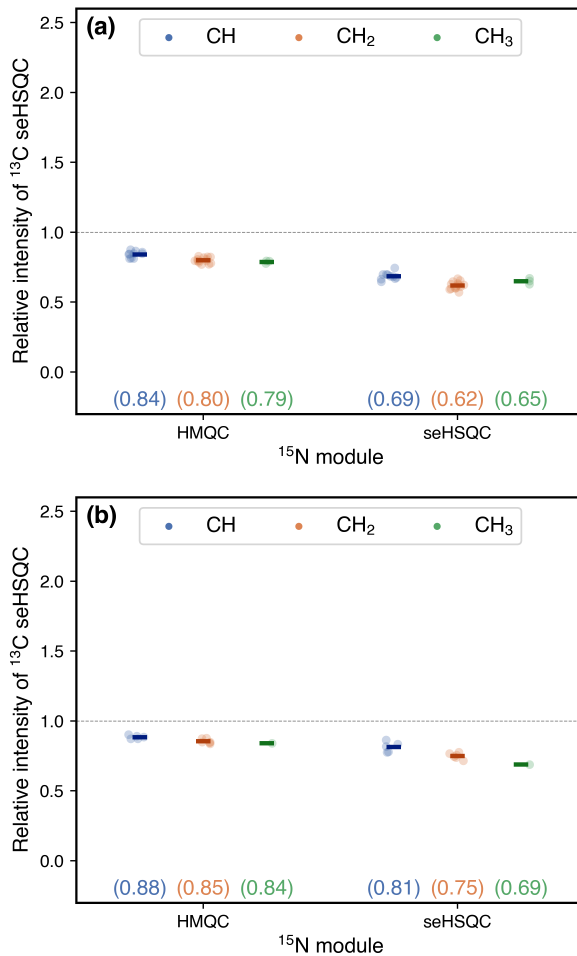


Figure S8: Signal intensities of the ^{13}C seHSQC in NOAH-3 XS^+C^c supersequences, normalised against a reference ^{13}C seHSQC taken from a NOAH-2 S^+C^c supersequence. The module X is either the ^{15}N HMQC (M) or the ^{15}N seHSQC (S_N^+); the numbers indicate the amount of $^1\text{H}^C$ magnetisation that is preserved by the ^{15}N module. (a) Using 40 mM gramicidin in DMSO- d_6 . (b) Using 50 mM zolmitriptan in DMSO- d_6 . Spectra were obtained on a 700 MHz Bruker AV III equipped with a TCI H/C/N cryoprobe.

7 ^{15}N HSQC and line broadening

For $^{15}\text{N}-^1\text{H}$ correlations, both the HMQC and the new seHSQC module are recommended as they keep the bulk magnetisation (both $^1\text{H}^{\text{C}}$ and $^1\text{H}^{\text{IX}}$) along $\pm z$ during the t_1 period. The HSQC module places this magnetisation in the xy -plane during t_1 , leading to J_{HH} evolution; consequently, the amount of bulk magnetisation “passed on” to the downstream modules decreases as the ^{15}N t_1 is increased. Since t_1 for each NOAH module is incremented in sync, this is manifested in downstream modules as a t_1 -dependent decrease in amplitude, or f_1 line broadening after Fourier transformation, as shown in Figure S9.

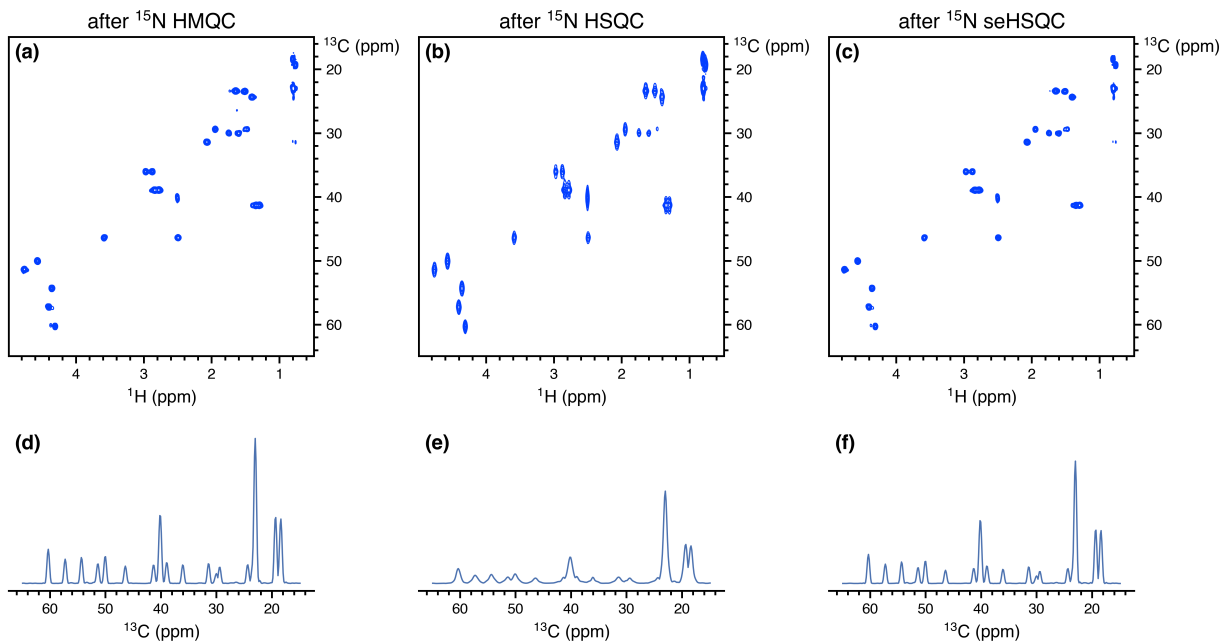


Figure S9: ^{13}C seHSQC spectra obtained from NOAH-3 XS $^+ \text{Cc}$ (^{15}N module + ^{13}C seHSQC + CLIP-COSY) supersequences. The ^{15}N spectral window was 30 ppm and 256 t_1 increments were collected, corresponding to an indirect-dimension ^{15}N acquisition time of 60.1 ms. (a) X = HMQC. (b) X = HSQC. (c) X = seHSQC. (d)–(f) Projections of spectra (a)–(c) onto the f_1 axis. Note the f_1 line broadening in (b) and (e). Spectra were obtained on a 700 MHz Bruker AV III equipped with a TCI H/C/N cryoprobe; the sample used was 40 mM gramicidin in DMSO- d_6 .

This line broadening also leads to a substantial sensitivity loss (for example, across all peaks, the ^{13}C seHSQC in Figure S9b has almost 65% lower sensitivity than that in Figure S9a). The extent of the line broadening depends on the acquisition time, and is particularly pronounced for long acquisition times, i.e. small ^{15}N spectral windows. In our experience, at ^{15}N acquisition times of ca. 5 ms the effect is almost indiscernible. Such a short acquisition time would lead to poor resolution in the ^{15}N dimension itself, which may or may not be tolerable. Of course, this issue can be entirely avoided by using either the HMQC or seHSQC.

8 Effect of lengthened gradients in ^{15}N modules

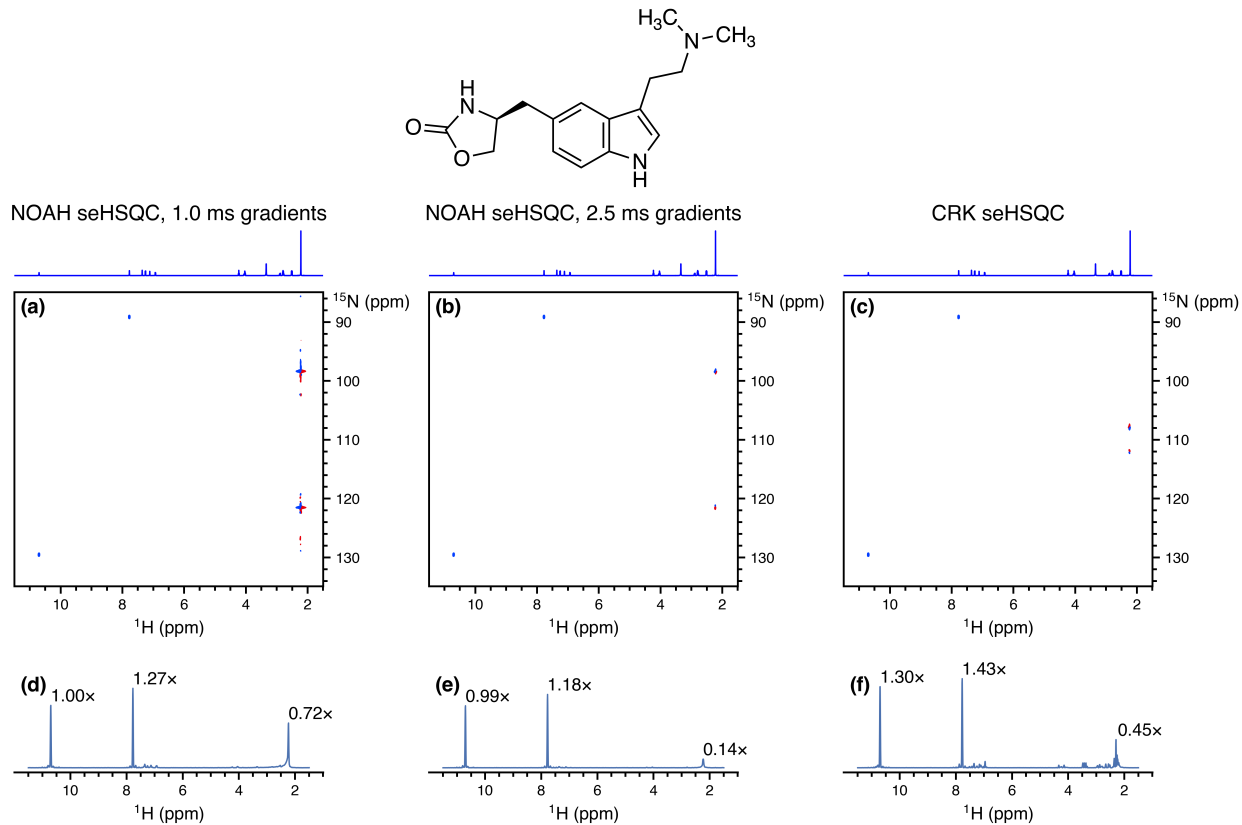


Figure S10: ^{15}N seHSQC spectra obtained using the NOAH and CRK implementations. The peaks at 7.8 and 10.7 ppm (^1H shifts) are genuine crosspeaks; the mixed-phase peaks at 2.2 ppm are artefacts. The 1D ^1H spectrum is shown above each of the 2D spectra in (a)–(c); the artefacts seen in the 2D correspond to the intense N -methyl groups at 2.2 ppm. (a) NOAH seHSQC, with original CTP gradients of 1 ms. (b) NOAH seHSQC, with longer CTP gradients of 1 ms. (c) Standalone CRK seHSQC with 1 ms CTP gradients (Bruker `hsqcetf3gpsi2` pulse programme). (d)–(f) Projections of spectra (a)–(c) onto the f_2 axis. The numbers indicate relative peak heights (normalised against the 10.7 ppm peak in (d)). Spectra were obtained on a 700 MHz Bruker AV III equipped with a TCI H/C/N cryoprobe; the sample used was 50 mM zolmitriptan in $\text{DMSO}-d_6$.

The lengthening of CTP gradients from 1 ms to 2.5 ms is aimed at cleaning up artefacts arising from bulk magnetisation that is not properly returned to $+z$ at the end of the sequence. Figure S10 shows exactly how effective this strategy is. In (d), where the CTP gradients have their original duration, the artefacts originating from the intense methyl groups have comparable intensity to the desired peaks. When the gradients are lengthened in (e), the crosspeak intensities are almost unaffected, whereas the artefacts are suppressed by a factor of 5 or more. Although this suppression is not complete, this should not be interpreted as a weakness of the new NOAH seHSQC module, as similar artefacts are also visible in the CRK seHSQC (f). Indeed, every ^{15}N – ^1H experiment we tested has at least *some* artefact intensity in this region.

9 Effect of k -scaling

The effect of k -scaling on the HMQC is shown in Figure S11. By decreasing the indirect dimension resolution, the f_1 linewidths of the peaks increase: this can lead to significant sensitivity enhancement for the HMQC (up to $2.7\times$), because J_{HH} splitting in the f_1 dimension is no longer resolved. The largest gains are observed for peaks where J_{HH} splitting is more visible; for the leftmost peak at $\delta_N = 128$ ppm which has no resolved J_{HH} splitting, only a more modest $1.7\times$ gain in sensitivity is attained.

For the seHSQC module, k -scaling on its own leads to far smaller sensitivity gains (Figure S12). Any increase in the total peak volume is almost completely offset by the f_1 broadening. Therefore, even at $k = 8$, the largest sensitivity gains that can be attained are $\sim 1.3\times$.

The use of linear prediction for spectra with $k > 1$ can, to a certain extent, compensate for the line broadening. This is less successful for the HMQC spectra (Figure S13). Although raw gains in peak height can be observed for all values of k , there is a corresponding decrease in the spectral quality, as evidenced by the f_1 multiplet structure being increasingly distorted. On the other hand, linear prediction performs well for the seHSQC spectra (Figure S14), where there is no multiplet structure in f_1 . Even the reconstruction with $k = 8$ has reasonable spectral quality: although the 2D spectrum (d) appears to have unusual peak shapes, this is merely the result of having the same contour levels as the $k = 1$ spectrum. The actual peaks are still clearly singlets, as can be seen from the projection in (h).

An additional example of successful k -scaling and linear prediction (with $k = 4$) can be seen in Section 11.

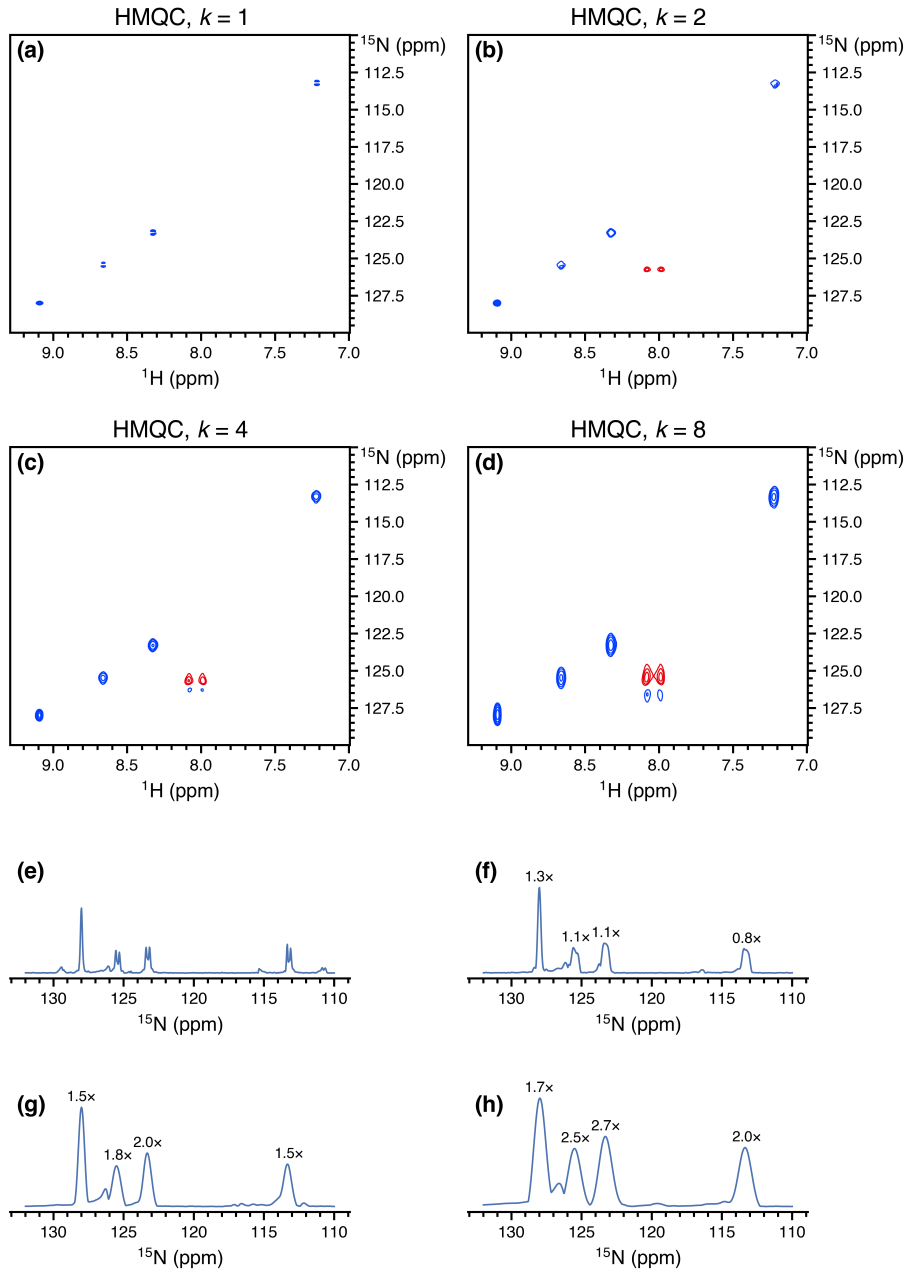


Figure S11: (HMQC without linear prediction.) ¹⁵N HMQC spectra (from NOAH-3 MS⁺C^c supersequences) obtained with various values of the scaling factor k . The peak at $\delta_{\text{H}} = 8.03$ ppm is a folded peak from the ornithine $\delta\text{-NH}_2$. (a) $k = 1$, with 256 t_1 increments and 2 scans per increment (denoted as 256 : 2). (b) $k = 2$, i.e. effectively 128 t_1 increments and 4 scans per increment (128 : 4). (c) $k = 4$ (64 : 8). (d) $k = 8$ (32 : 16). (e)–(h) Projections of 2D spectra in (a)–(d) onto the f_1 axis, shown at the same noise level. Numbers indicate peak heights relative to the $k = 1$ HMQC spectrum. Spectra were obtained on a 700 MHz Bruker AV III equipped with a TCI H/C/N cryoprobe; the sample used was 40 mM gramicidin in DMSO-*d*₆.

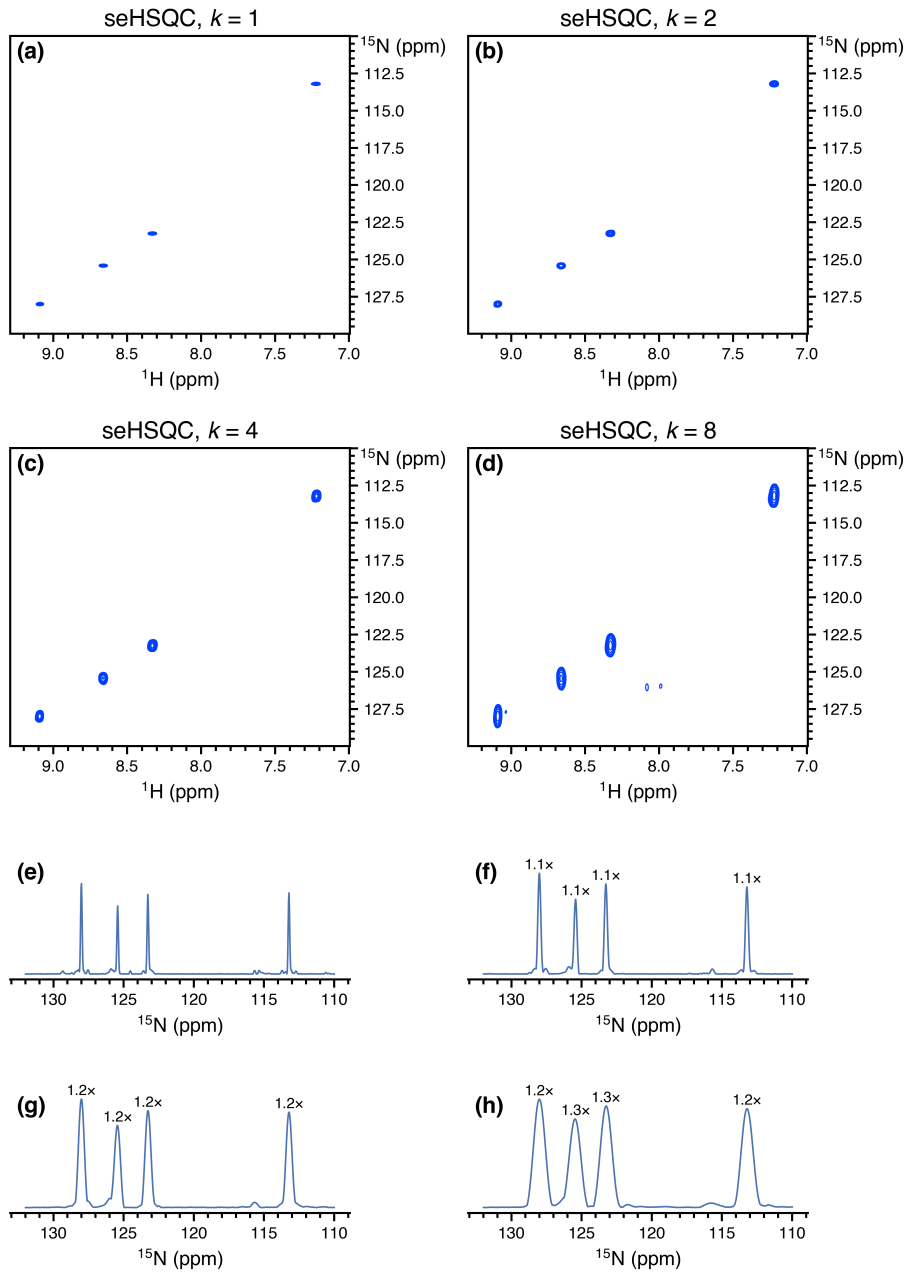


Figure S12: (seHSQC without linear prediction.) ^{15}N seHSQC spectra (from NOAH-3 $\text{S}_\text{N}^+\text{S}^+\text{C}^\text{c}$ super-sequences) obtained with various values of the scaling factor k . The peak at $\delta_\text{H} = 8.03$ ppm is a folded peak from the ornithine δ -NH₂. (a) $k = 1$ (256 t_1 increments, 2 scans each). (b) $k = 2$ (128 : 4). (c) $k = 4$ (64 : 8). (d) $k = 8$ (32 : 16). (e)–(h) Projections of 2D spectra in (a)–(d) onto the f_1 axis, shown at the same noise level. Numbers indicate peak heights relative to the $k = 1$ seHSQC spectrum. Spectra were obtained on a 700 MHz Bruker AV III equipped with a TCI H/C/N cryoprobe; the sample used was 40 mM gramicidin in DMSO-*d*₆.

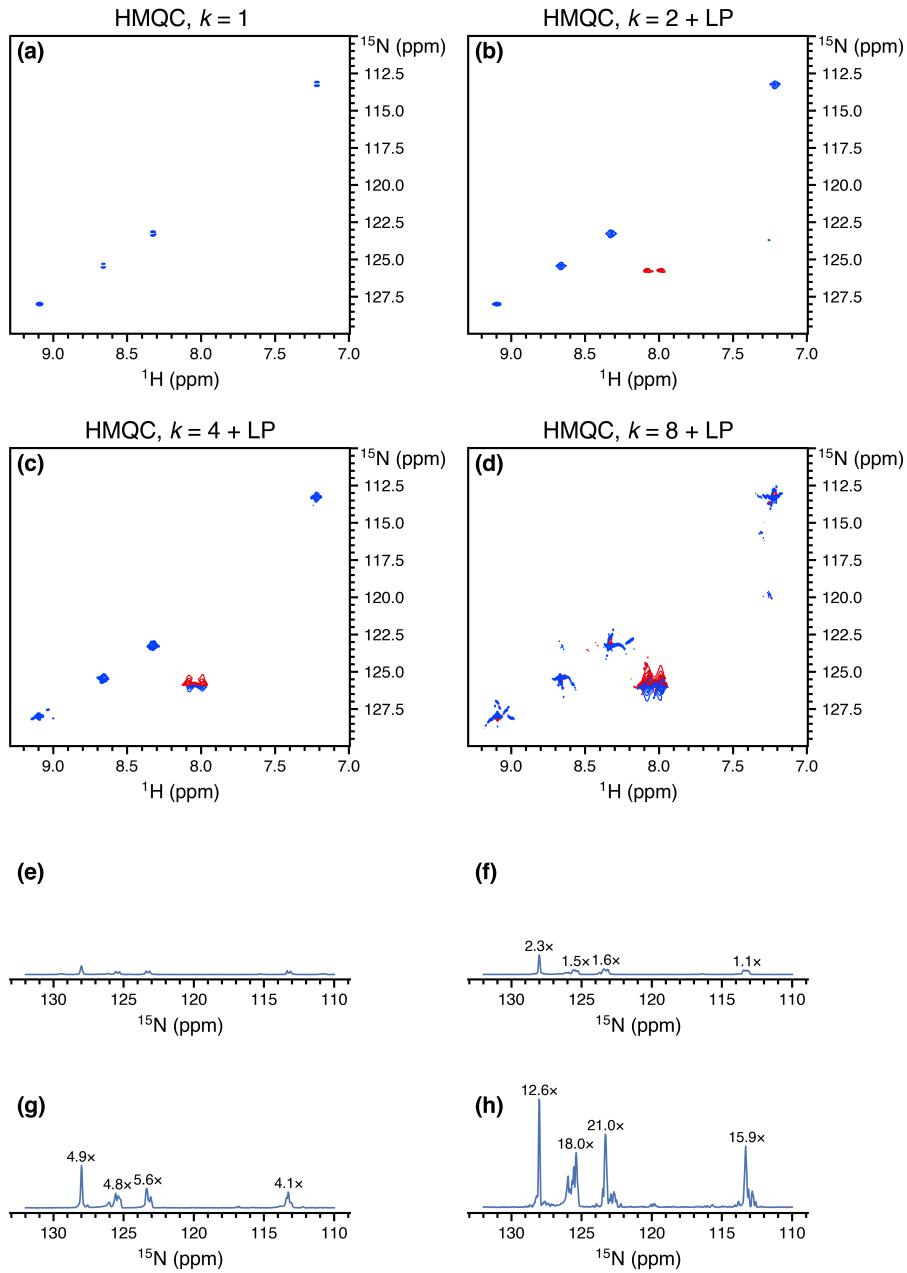


Figure S13: (HMQC with linear prediction.) ^{15}N HMQC spectra (from NOAH-3 MS⁺C^c supersequences) obtained with various values of the scaling factor k , after linear prediction up to 512 complex points in f_1 . The peak at $\delta_{\text{H}} = 8.03$ ppm is a folded peak from the ornithine $\delta\text{-NH}_2$. (a) $k = 1$ (256 : 2). Note that this spectrum is the same as in Figure S11a. (b) $k = 2$ (128 : 4). (c) $k = 4$ (64 : 8). (d) $k = 8$ (32 : 16). (e)–(h) Projections of 2D spectra in (a)–(d) onto the f_1 axis, shown at the same noise level. Numbers indicate peak heights relative to the $k = 1$ HMQC spectrum. Spectra were obtained on a 700 MHz Bruker AV III equipped with a TCI H/C/N cryoprobe; the sample used was 40 mM gramicidin in DMSO-*d*₆.

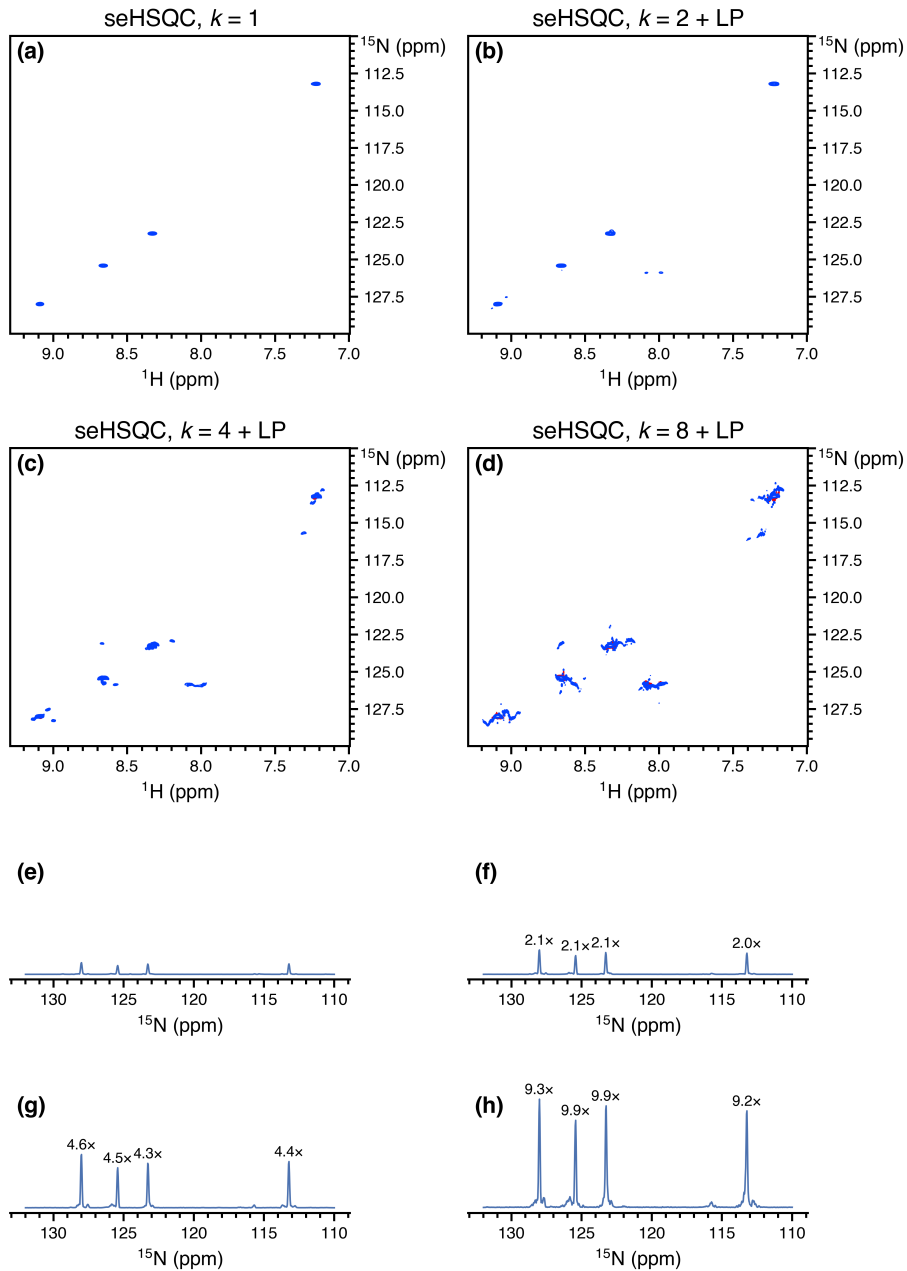


Figure S14: (seHSQC with linear prediction.) ¹⁵N seHSQC spectra (from NOAH-3 S_N⁺S⁺C^c supersequences) obtained with various values of the scaling factor k , after linear prediction up to 512 complex points in f_1 . The peak at $\delta_H = 8.03$ ppm is a folded peak from the ornithine $\delta\text{-NH}_2$. (a) $k = 1$ (256 : 2). Note that this spectrum is the same as in Figure S12a. (b) $k = 2$ (128 : 4). (c) $k = 4$ (64 : 8). (d) $k = 8$ (32 : 16). (e)–(h) Projections of 2D spectra in (a)–(d) onto the f_1 axis, shown at the same noise level. Numbers indicate peak heights relative to the $k = 1$ seHSQC spectrum. Spectra were obtained on a 700 MHz Bruker AV III equipped with a TCI H/C/N cryoprobe; the sample used was 40 mM gramicidin in DMSO-*d*₆.

10 HSQC-TOCSY/HSQC sensitivity comparisons

The signal intensities for the NOAH-3 S^TSC^c (HSQC-TOCSY + HSQC + CLIP-COSY) supersequences can be more conveniently measured by omitting the DIPSI-2 isotropic mixing in the HSQC-TOCSY supersequence, leading to a NOAH-3 SSC^c (HSQC + HSQC + CLIP-COSY) supersequence. This allows us to compare the different versions of double-HSQC sequences, as the two HSQC modules can be implemented either using the MFA approach, or the new ASAP/NOAH approach based on Ernst angle excitation in the first module. In the latter implementation, the parameter f can be varied between 0.4 and 1; it represents the proportion of ¹H^C magnetisation used in the first HSQC, as described in the main text. Furthermore, to boost the sensitivity of the second HSQC module in the NOAH supersequences, the new seHSQC module can be used in its place.

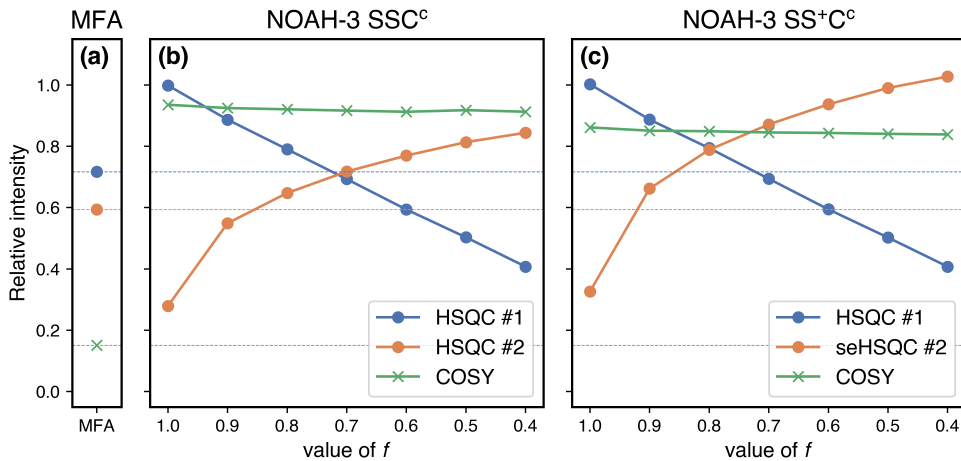


Figure S15: Sensitivities of HSQC and CLIP-COSY modules when used as part of a SSC^c-type supersequence, with both the NOAH and MFA implementations of the two HSQC modules. Intensities are calculated relative to the HSQC and CLIP-COSY modules in a standard NOAH-2 SCc supersequence (averaged over all peaks). (a) Sensitivity of the MFA implementation (i.e. a MFA double HSQC experiment immediately followed by a CLIP-COSY). Horizontal dashed lines at these levels are drawn across all subplots to guide the eye. (b) Sensitivity of NOAH-3 SSC^c modules as a function of f . Note that at $f = 0.8$, all of the NOAH spectra have a greater average sensitivity than their MFA counterparts. (c) Sensitivity of NOAH-3 SS^{+C}^c modules as a function of f . Spectra were obtained on a 700 MHz Bruker AV III equipped with a TCI H/C/N cryoprobe; the sample used was 40 mM andrographolide in DMSO-*d*₆.

Figure S15 may be understood in the following way:

- The MFA HSQC sensitivities (in (a)) are approximately half that of a standard CRK seHSQC, with the second HSQC having slightly lower sensitivity. This is discussed in ref. 17 of the main text.
- The sensitivity of the first NOAH HSQC (blue in (b) and (c)) is generally equal to f , sup-

porting the interpretation of f as the fraction of $^{13}\text{C}-^1\text{H}$ magnetisation excited in the first HSQC.

- The sensitivity of the second NOAH HSQC (orange in (b)) arises from whatever is *not* used by the first HSQC, plus any magnetisation that relaxes during the FID of the first HSQC. As f is decreased, the former contribution increases and the latter tapers off. This is true for the seHSQC as well (orange in (c)), except that there is a uniform boost in sensitivity for all values of f . This sensitivity improvement mainly applies to CH groups, as discussed in the main text.
- The MFA COSY sensitivity (green) is substantially lower ($\sim 15\%$) because the bulk magnetisation is dephased by the previous modules, whereas in the NOAH approach it is (largely) preserved.

It remains to evaluate the impact of adding DIPSI-2 mixing in one of the HSQC modules on the remaining modules in the supersequence. This depends on whether the HSQC-TOCSY module is placed first ($S^T\text{SC}^c$ or $S^T\text{S}^+C^c$) or second (SS^TC^c) in the sequence. Since the seHSQC module does not preserve unused $^1\text{H}^C$ magnetisation, the HSQC-TOCSY in a hypothetical $S^+S^TC^c$ supersequence will have greatly reduced sensitivity. On the other hand, placing the HSQC-TOCSY sequence first allows the seHSQC module to be used subsequent to this; we therefore consider only the permutations where the HSQC-TOCSY goes first.

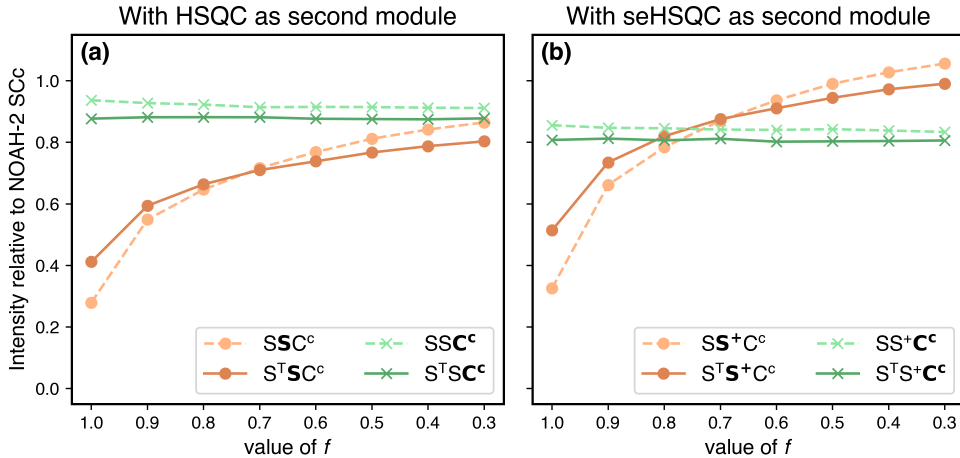


Figure S16: Comparison of signal intensities of second (HSQC or seHSQC) and third (CLIP-COSY) modules in the $S^T\text{SC}^c$ and $S^T\text{S}^+C^c$ supersequences, versus their intensities in the SSC^c and SS^+C^c sequences, as a function of the parameter f . The solid, darker lines indicate the supersequences beginning with the HSQC-TOCSY, whereas the dashed, lighter lines indicate the supersequences beginning with the HSQC (the latter are the same graphs as in Figure S15). **(a)** With the HSQC as the second module. **(b)** With the seHSQC as the second module. Spectra were obtained on a 700 MHz Bruker AV III equipped with a TCI H/C/N cryoprobe; the sample used was 40 mM andrographolide in $\text{DMSO}-d_6$.

It can be seen from Figure S16 that the introduction of DIPSI-2 mixing leads to a very small drop (< 10%) in the amount of $^1\text{H}^{1\text{C}}$ magnetisation preserved for the COSY module. On the other hand, the HSQC (and seHSQC) sensitivities follow largely the same trend as before. For values of f above 0.7 (where relatively little $^1\text{H}^{1\text{C}}$ magnetisation is preserved for these modules), the DIPSI-2 mixing helps to replenish some of this magnetisation. As f decreases, this effect becomes smaller, and at small f it even leads to a reduction in signal intensity. As discussed in the main text, since the HSQC-TOCSY has a lower intrinsic sensitivity than the (se)HSQC, we recommend using a large value of f , such as 0.9. This does not compromise the HSQC-TOCSY intensity by much, and at the same time yields either a HSQC with $\sim 65\%$ of its original sensitivity, or a seHSQC which has $\sim 80\%$ of the sensitivity of a standard NOAH HSQC.

Finally, we note that because a significant proportion of the HSQC signal derives from $^1\text{H}^{1\text{C}}$ relaxation during the HSQC-TOCSY FID, use of a larger acquisition time (AQ) can potentially boost the HSQC sensitivity even further. The experiments shown above were carried out with a relatively short AQ of 73 ms. However, bear in mind that the high duty cycle associated with broadband ^{13}C decoupling can potentially cause hardware damage if applied for too long, especially given that the supersequences described here have two consecutive ^{13}C -decoupled modules.

11 Other example spectra

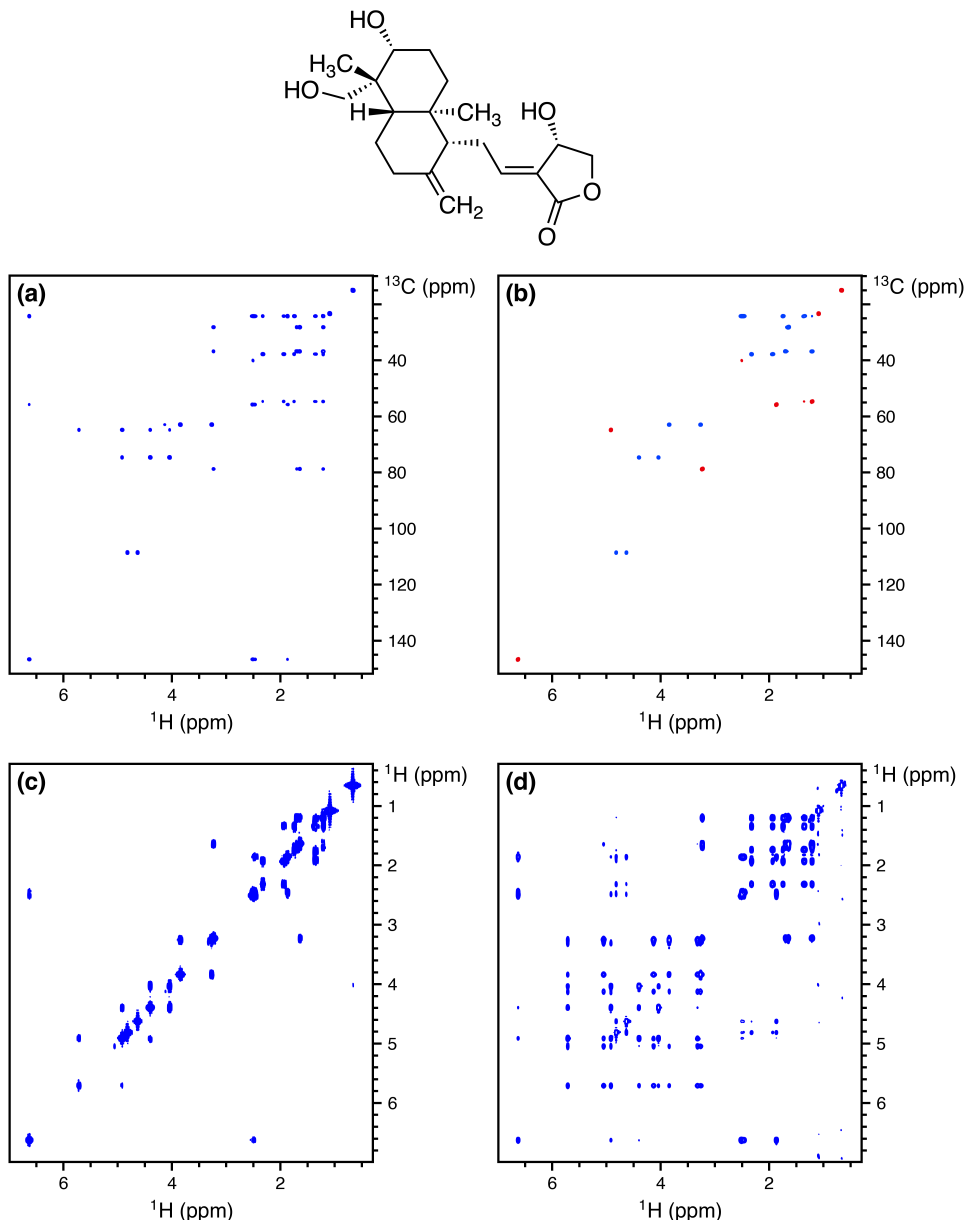


Figure S17: 2D spectra acquired using the NOAH-4 S^TS+CT supersequence. 256 t_1 increments were used with 2 scans per increment, leading to a total experiment time of 17 minutes and 32 seconds. This represents a 3.25× time saving relative to conventional acquisition of each of the four spectra with the same parameters, which would take a total of 57 minutes and 3 seconds. (a) HSQC-TOCSY (30 ms mixing time, $f = 0.9$). (b) Multiplicity edited seHSQC. (c) COSY. (d) TOCSY (60 ms mixing time). Spectra were obtained on a 700 MHz Bruker AV III equipped with a TCI H/C/N cryoprobe; the sample used was 40 mM andrographolide in DMSO-*d*₆.

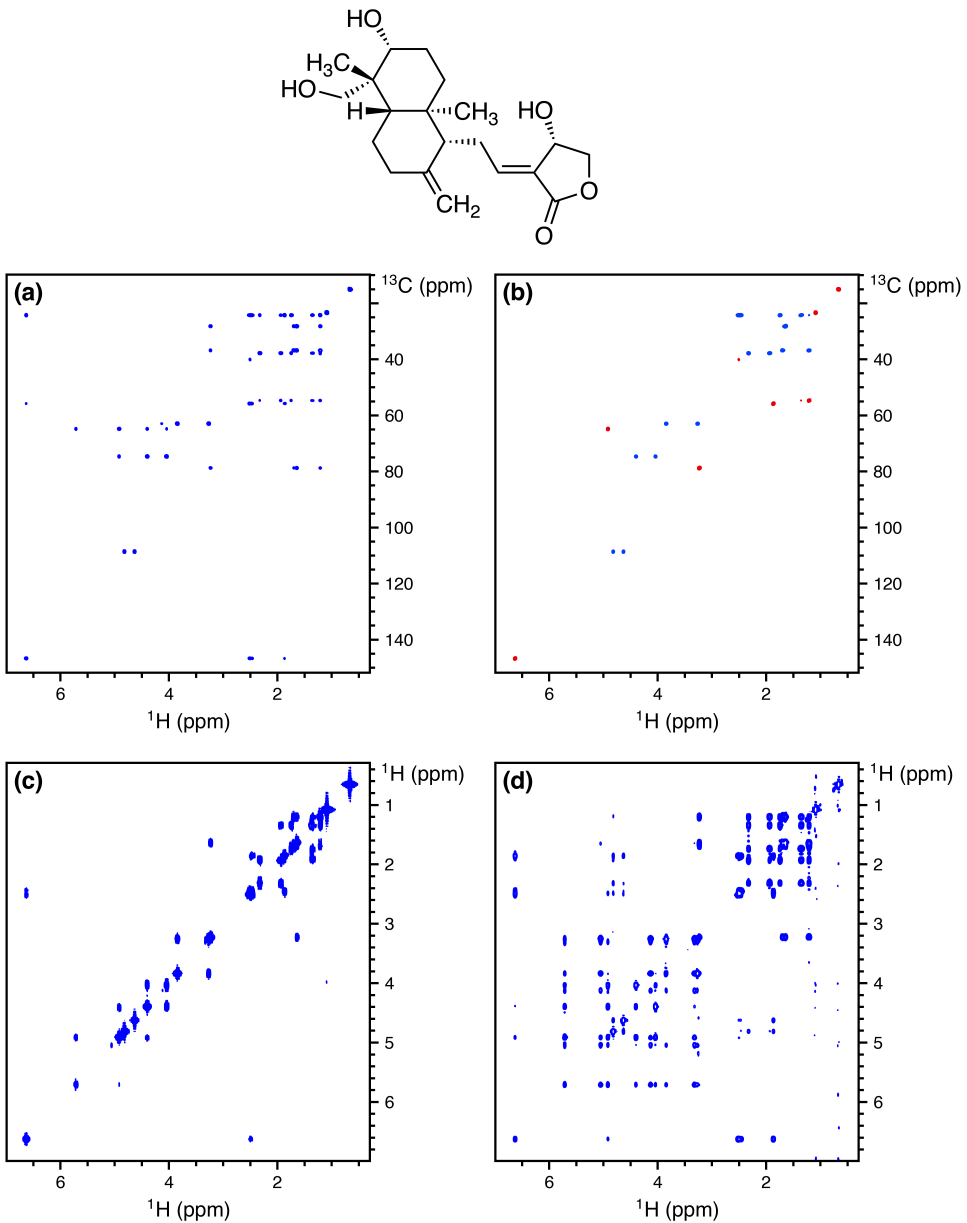


Figure S18: 2D spectra acquired using the NOAH-4 S^TS⁺CT supersequence with 50% non-uniform sampling for all modules. All other parameters are the same as in Figure S17. The experimental time was 9 minutes and 1 second. **(a)** HSQC-TOCSY (30 ms mixing time, $f = 0.9$). **(b)** Multiplicity edited seHSQC. **(c)** COSY. **(d)** TOCSY (60 ms mixing time). Spectra were obtained on a 700 MHz Bruker AV III equipped with a TCI H/C/N cryoprobe; the sample used was 40 mM andrographolide in DMSO-*d*₆.

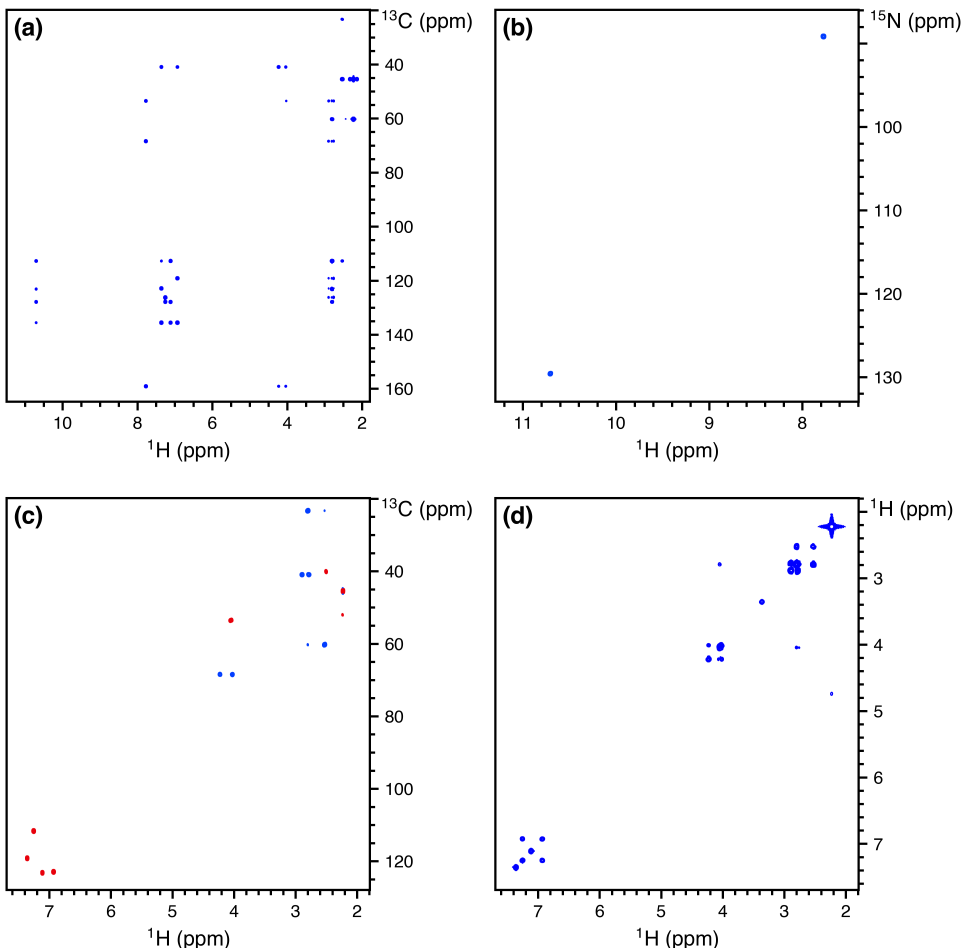
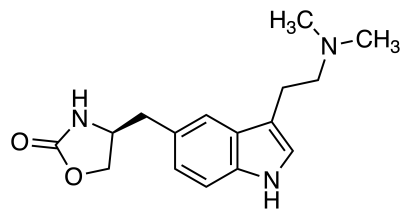


Figure S19: 2D spectra acquired using the NOAH-4 BS_N⁺S⁺C supersequence. 256 t_1 increments were used with 2 scans per increment, leading to a total experiment time of 17 minutes and 32 seconds. This represents a 3.22× time saving relative to conventional acquisition of each of the four spectra with the same parameters, which would take a total of 56 minutes and 28 seconds. (a) HMBC. (b) ¹⁵N seHSQC with $k = 4$, linear projected to 512 complex points. (c) Multiplicity edited ¹³C seHSQC. (d) Magnitude-mode COSY (Bruker qf mode). Spectra were obtained on a 700 MHz Bruker AV III equipped with a TCI H/C/N cryoprobe; the sample used was 50 mM zolmitriptan in DMSO-*d*₆.

12 Pulse programmes

- SCc
- SpCc
- MSpCc
- SnSpCc
- SpnSpCc
- SSCc
- SSpCc
- StSCc
- StSpCc
- StSpCT
- BSpnSpCqf

13 Processing scripts

We basically need everything, including the new version of NUS.